IN-34
137057
P.45

NASA Technical Memorandum 105865

Numerical Study of Mixing of Two Fluids Under Low Gravity

Walter M.B. Duval
Lewis Research Center
Cleveland, Ohio

November 1992

(NASA-TM-105865) NUMERICAL STUDY OF MIXING OF TWO FLUIDS UNDER LOW GRAVITY (NASA) 45 p

N93-14914

Unclas

G3/34 0137057

NASA

Numerical Study of Mixing of Two Fluids Under Low Gravity

Walter M.B. Duval

NASA Lewis Research Center
Cleveland, Ohio 44135

ABSTRACT

The mixing characteristic of two fluids inside a cavity due to buoyancy driven flow fields for low gravity conditions is investigated via numerical experiments. The buoyancy driven flow, depending on the parametric region, stretches and deforms the material interface into a wave morphological pattern. The morphological pattern affects the resulting stratification thickness of the mixed region. Three basic mixing regimes occur: convective, diffusive, and chaotic. In the convective regime, an overturning motion occurs which gives rise to a stable wave formation. This wave oscillates and its decay leads to a stable stratification. Whereas, in the diffusive regime, the length of the interface remains constant while mixing occurs. This limiting behaviour is very important to materials processing in space, and it admits a closed form solution corresponding to vanishing convective terms which agrees with computational results. Finally in the chaotic regime, the material interface continuously stretches and folds on itself similar to a horseshoe map. The length of stretch of the interface increases exponentially. Internal wavebreaking occurs for this case. This wavebreaking generates local turbulence, and provides an effective mechanism for mixing.

August 21, 1992

Numerical Study of Mixing of Two Fluids Under Low Gravity

Walter M.B. Duval

NASA Lewis Research Center
Cleveland, Ohio 44135

1. Introduction.

Materials processing in low earth orbit has recently received attention because of intrinsic advantages over ground based processes. These advantages include the control of delicate processes, and stem from the low buoyancy driven flows in bulk fluids which occur in various phenomena, such as phase transformations during crystal growth, and fluid-fluid interactions for mixing processes. Because of the inherent coupling of temperature and concentration fields in materials processing, uncontrolled buoyancy flows can have deleterious effects on many phenomena. Some examples include striation effects in crystal growth, and convective effects masking the measurement of diffusion coefficient. The low gravity condition of space provides a controlled environment where buoyancy driven flows can be minimized and processes can potentially attain a greater degree of optimization than that obtainable on earth.

Under low gravity environment many phenomena that are adversely affected due to buoyancy flows can be easily carried out in space without being masked by convection. One such case is the measurement of self and interdiffusion coefficients. As pointed out by Froberg, Kraatz, and Wever (1987) the elimination of convective effects yields measurements of diffusion coefficients with an accuracy of 10 to 50 times better than those made in ground laboratories. Another example is the counterdiffusion process, see Gerbi et. al (1986), for solution crystal growth. This process involves mass transport of liquids through multiple chambers in order to grow crystals. Galster, and Nielsen (1984) have pointed out that this process has benefited from microgravity because of the minimization of convective effects. In comparison to the crystals grown on earth, the results of their space experiments show that higher quality crystals resulted, free from striation effects. In addition, Radcliffe et al. (1988) have shown, through their space experiments, the parametric range under which liquids are mixed by convective effects. They have also delineated the conditions under which mixing occurs by mass diffusion alone without significant convection. These experiments were carried out in closed chambers without any photographic device to capture the details of the fluid dynamics.

We present a model problem to study mixing of two fluids inside a closed cavity under low gravity conditions which shows the fluid dynamic details. Similar to many phenomena in materials processing, the mixing is driven by buoyancy forces. This is unlike many industrial mixing phenomena, as presented by Nagata (1975) and Uhl & Gray (1966), that are induced by mechanical devices. This model problem allows us to determine parametric ranges under which convective effects driven by buoyancy forces play a predominant role in mixing, and it also allows us to delineate the conditions for which diffusive mixing can be expected.

Mixing due to buoyancy generated flow fields are of interest in many materials processing phenomena. Closely related to our model problem is the mixing of two different fluids by Rayleigh-Taylor instability. Recently, Andrews and Spalding (1990) have designed an experiment to study two-dimensional mixing by Rayleigh-Taylor instability using both photographic means and an imaging based measurement system. They investigated both one dimensional plane mixing and tilted two-dimensional experiments. In the one-dimensional (no-tilt) experiment they show that the mixing region expands in proportion to gt^2. Whereas, in the tilted ($55^{\prime}$ and $3^{\circ}21^{\prime}$) two-dimensional experiments, a large scale two-dimensional overturning motion was superimposed on the Rayleigh-Taylor mixing process. The large scale motion stretched the mixing interface and caused its width to be reduced. In the early stages of the experiments the width of the interface is approximately the same for both cases. Because of the stretching of the interface in the two-dimensional case, to preserve continuity the width of the interface contracts as time increases. These phenomena of mixing which involves stretching and folding of material lines have been described more generally by Ottino (1982). Our model problem has some similarity to the tilted experiments of Andrews and Spalding. In our case we consider a model problem which corresponds to a 90^0 tilt case which can be practically achieved only under microgravity conditions. This case is of interest because processes for solution crystal growth use a similar configuration.

At its fundamental level, fluid mixing consists of stretching and folding of material lines by a flow field to achieve a reduction of length scales. This is accompanied by thinning of materials volumes and dispersion throughout space; in addition diffusion of mass and heat may also take place. The flow field may be induced by either mechanical means or it may be caused by buoyancy forces in the case of materials processing. The fluids may be either miscible or immiscible. The interface between the two fluids, as defined by Aref and Tryggvason (1984), may be respectively passive or active. In the case of passive interfaces, the boundary between the two fluids serves

as a marker of the flow and the motion may be topological. Whereas in the case of active interfaces, there is interaction of the interface with the flow field to modify it. A framework for the description of fluid interfaces as a material surface to describe mechanical mixing have been developed by Ottino, Ranz, and Macosko (1981) using continuum mechanical arguments. They consider the case of immiscible materials with clearly defined interfaces and negligible interfacial tension. A metric to quantify the state of mixing, Ottino, Ranz, and Macosko (1979), is the striation thickness defined as $s=1/a_v$, where a_v is the interfacial area density. In the case where interdiffusion occurs at the interface, s has a distributed rather than an average value. Thus in the case of miscible fluids, the state of mixing is quantified by uniformity of the concentration field. In our model we consider two liquids with passive interfaces and negligible interfacial tension. We show the effect of buoyancy flow fields on the kinematics of interfacial deformation, and also show the parametric range under which mixing can be effective. While this work discusses the effect of steady acceleration, time dependent acceleration or g-jitter, has been considered by Duval & Jacqmin (1990) and Duval (1992).

This paper is organized as follows: in section 2, we formulate the model problem and its characteristic parameters are delineated from scaling arguments. In section 3 we discuss the solution technique. In section 4 we present the parametric range to be studied and show the details of the three most basic mixing regimes for buoyancy generated flows inside cavities, namely: convective, chaotic, and diffusive. Measures to quantify mixing are also shown. We conclude by drawing inferences to related works in the literature.

2. Formulation

By virtue of its significance in materials processing, we consider the situation shown in Figure 1, where the two liquids meet at a sharp density interface inside a rectangular cavity. These two liquids are treated as Boussinesq fluids with properties approximated as average. The physical situation is approximated as:

$$\nabla\cdot\vec{V}^* = 0$$

$$\bar{\rho}\frac{D\vec{V}^*}{Dt^*} = -\nabla p^* + \bar{\mu}\nabla^2\vec{V}^* + \rho\vec{g}$$

$$\frac{DC^*}{Dt^*} = \tilde{D}_{lr}\,\nabla^2 C^*$$

over the region inside the cavity.

The initial and boundary conditions are:

$$t = 0 \qquad C^*(x,y,t) = \begin{cases} 1 & 0 \le x < L/2 \\ .5 & x = L/2 \\ 0 & L/2 < x \le L \end{cases}$$

$$t > 0 \qquad \vec{V}^* = 0 \text{ on } \Gamma, \text{ no slip}$$

$$\nabla C^* \cdot \vec{n} = 0 \text{ on } \Gamma, \text{ condition of impermeability}$$

where

$$\rho = \bar{\rho}(1 + \beta \Delta C)$$

$$\beta = \frac{1}{\bar{\rho}} \frac{\partial \rho}{\partial C}$$

$$\vec{g} = n g_o \vec{j} \ .$$

In the above equations ΔC represents the concentration difference between the left and right side of the cavity. Γ denotes the boundary of the cavity, and $\vec{n}$ its normal. The factor n multiplying the gravitational acceleration constant, g_o, is a ratio by which gravity can be reduced to represent typical conditions on a space shuttle, and $\vec{j}$ is the unit vector in the vertical direction. The boundary conditions along the cavity walls are no slip and impermeability of the concentration field. The overbar and * denote, respectively, average and dimensional quantities. Subscripts l and r denote left and right, respectively. The viscosity and diffusion coefficient are independent of concentration.

In the initial condition, the left and right fluids are assigned distinct values of concentration, the interface between the two fluids is treated as a tracer. This tracer, according to Ottino (1982), is a hypothetical material that moves everywhere with the mean velocity of the mixture. Thus, the distinct value of C=.5 represents a material line in terms of particles of tracer moving with the mean velocity. This material line does not diffuse, but it is permeable to the diffusion of species. Since we are allowing for interdiffusion, the spreading of concentration lines with values ranging from .9 to .6 on the left side of the interface, and .4 to .1 on the right side will give an indication of mass transport by interdiffusion. Even though the equation of an interface is strictly $DC/Dt = 0$, we can still talk about an interface if $DC/Dt \neq 0$ provided that we can follow a distinct hypothetical material line in the region of interest. Thus, within a non-material region which allows for diffusion, distinct set of particles with the same

identity can be treated like a material line or surface.

To study the physics of the problem, the above set of equations were recast into vorticity- stream function form with the following dimensionless numbers defined as:

$$x = \frac{x^*}{L} \qquad y = \frac{y^*}{H} \qquad u = \frac{u^*}{U_c} \qquad v = \frac{v^*}{U_c} \qquad t = \frac{t^*}{T}$$

$$C = \frac{C^* - C_r^*}{C_l^* - C_r^*} \qquad \Psi = \frac{\Psi^*}{U_c H} \qquad \zeta = \frac{\zeta^* H}{U_c}$$

where

$$u^* = \frac{\partial \Psi^*}{\partial y^*} \qquad v^* = -\frac{\partial \Psi^*}{\partial x^*} \qquad \zeta^* = \frac{\partial v^*}{\partial x^*} - \frac{\partial u^*}{\partial y^*}$$

With these scales, the continuity, momentum, and species continuity become:

$$Ar^2 \frac{\partial^2 \Psi}{\partial x^2} + \frac{\partial^2 \Psi}{\partial y^2} = -\zeta$$

$$\frac{\partial \zeta}{\partial t} + Gr\left[Ar \; u\frac{\partial \zeta}{\partial x} + v\frac{\partial \zeta}{\partial y} \right] = \left[Ar^2 \frac{\partial^2 \zeta}{\partial x^2} + \frac{\partial^2 \zeta}{\partial y^2} \right] + Ar\frac{\partial C}{\partial x}$$

$$\frac{\partial C}{\partial t} + Gr\left[Ar \; u\frac{\partial C}{\partial x} + v\frac{\partial C}{\partial y} \right] = \frac{1}{Sc}\left[Ar^2 \frac{\partial^2 C}{\partial x^2} + \frac{\partial^2 C}{\partial y^2} \right]$$

The characteristic time, T, and velocity, U_c, are scaled with the viscous diffusion and buoyancy forces respectively, i.e., $T = \frac{H^2}{\bar{\nu}}$ and $U_c = \frac{\Delta \rho n g_o}{\bar{\rho}} \frac{H^2}{\bar{\nu}}$. Three governing parameters arise from the dimensionless form of the equations, namely: the Grashof number (Gr), the Schmidt number (Sc), and the aspect ratio (Ar) of the cavity. These parameters are defined as:

$$Gr = \frac{\Delta \rho n g_o}{\bar{\rho}} \frac{H^3}{\bar{\nu}^2} \qquad Sc = \frac{\bar{\nu}}{\bar{D}_{lr}} \qquad Ar = \frac{H}{L}$$

The Grashof number is the ratio of buoyancy to viscous forces, the Schmidt number indicates the diffusion of viscosity relative to that of mass, and the aspect ratio denotes the ratio of the height of the cavity to its length. Since we have a nonhomogeneous media, a vorticity creation term arises. According to the dimensionless set of field equations, the evolution of the interface and flow field can be modified by the aspect ratio. For very low aspect ratios ($Ar \rightarrow 0$), the horizontal components of the field equations become negligible in comparison to the vertical components. This corresponds to the case of a very long, narrow, horizontal cavity. In this limit, the buoyancy force in the Grashof number which gives rise to flow, becomes very small

and viscous diffusion dominates. In addition, the vorticity creation term becomes negligible, thus the flow field is decoupled from the concentration field. And the limiting case of one-dimensional mixing via interdiffusion with negligible convection due to buoyancy effects is obtained. In contrast, the other limiting case of a very tall vertical cavity ($Ar \to \infty$), indicates dominance of the horizontal components in the field equations. The flow field is driven by buoyancy forces and the creation of vorticity term becomes important. The nonlinear convective terms in the horizontal direction dominates for this case. Thus, mixing is more efficient due to the overwhelming influence of the buoyancy force. This is in contrast to the case for the horizontal narrow cavity.

Even though the characteristic time in the scaling of the field equations is based on molecular viscous diffusion, T_ν, two other time scales also exist. These time scales are based on effects of buoyancy, T_b, and molecular mass diffusion, T_D. They are defined as:

$$T_b = \frac{1}{\sqrt{\frac{\Delta\rho}{2\bar{\rho}}\frac{ng_o}{H}}} \quad \text{and} \quad T_D = \frac{H^2}{\tilde{D}_{lr}}$$

Note that the Atwood number, $At = \Delta\rho/2\bar{\rho}$, which commonly appears as a factor in the equation for growth rate of perturbations for Rayleigh-Taylor instability also occurs above. T_b represents the characteristic time it takes a particle to travel a distance H neglecting drag effects, it is also a measure of the short time events of the phenomena. It can also be shown that $T_b = N^{-1}$, where N is the buoyancy frequency that commonly appears in the definition of Richardson number (i.e. $Ri = N^2/(\partial u/\partial y)^2$. The third time scale, T_D denotes the long time mixing events leading toward equilibrium or a homogeneous mixture when convective effects are vanishingly small. For a given binary system subjected to various gravitational levels, the viscous and mass diffusion time scales are fixed. However, the buoyancy time scale approaches infinity, $T_b \to \infty$ as $n \to 0$, also $Gr \to 0$. This corresponds to the diffusive limit where buoyancy forces are no longer effective. In this case T_D would be the appropriate time scale. When $T_b \to 0$ ($Gr \to \infty$) which corresponds to ground based accelerated conditions then the proper time scale is T_b, since the mixing phenomena would occur relatively fast. However, when T_b lies between these limiting cases, a good overall time scale (as will be shown in our numerical examples) is T_ν. For the diffusive limit $Gr \to 0$, even if we scale with T_ν, the proper scale, T_D, as will be shown, is recovered from the solution.

Though the limiting behavior of the vertical and horizontal cavity allows qualitative interpretation of the scaled field equations and indicates how simplification can be

obtained, for practical materials processing inside cavities, that degree of freedom is often not available. One is limited to work with finite cavity sizes. Thus, it is necessary to deal with the full complexity of the problem, which is governed by the set of equations. Note that for a square cavity, the problem is governed principally by the Grashof number. If the gravitational field can be reduced to sufficiently small values, the nonlinear advective terms in the field equations can become negligible. In this case, irrespective of the magnitude of the aspect ratio, one-dimensional mixing via interdiffusion can be obtained. Therein, lies the importance of microgravity to materials processing.

3. Solution Technique

In this model problem, by virtue of the initial configuration, buoyancy forces will cause the onset of convective flow fields however small. The convective flow field may or may not deform the interface. This will depend on the magnitude of the Grashof (Gr) number. Furthermore, the importance of the nonlinear terms in the field equations is also dependent on the magnitude of Gr. Hence, it is imperative to choose a numerical technique which is suitable to resolve the sharp interface region, and have the property of handling discontinuities. One such method is the Flux Corrected Transport (FCT) developed by Boris & Book (1973) and Book (1981). The FCT method is known for its ability to resolve steep gradients such as shocks and discontinuities. One of the drawbacks of applying finite difference techniques to buoyancy flows dominated by nonlinear advective terms is the numerical oscillation that occurs because the transported component (in our case the concentration component) can become negative over the domain of computation. The FCT method assures positivity of the concentration component, thus eliminating false numerical oscillation. Comparison of the FCT method to compute the nonlinear advective terms in the concentration field equation with other techniques such as upwind differencing and central differencing assured us of its excellent ability to track interfaces.

The set of field equations is solved by direct finite difference methods. The stream function equation is solved using a Poisson solver with direct matrix inversion. The time and spatial diffuse terms are discretized respectively, using third order Adams Bashforth scheme and central differencing. Most importantly we use the FCT method to compute the nonlinear advective terms in the species concentration equation. Lastly, the vorticity boundary condition is computed using a method suggested by Roache (1972, pp 139-174). Numerical studies on the effect of grid size show that a 36×36 mesh is sufficient to resolve the large scale details of the flow field for the cavity

sizes considered. The time step selected is small enough to insure stability of the calculations.

4. Discussions and Numerical Results

4.1 Parametric range

The range of conditions considered is dictated by practical achievable conditions in space with typical cavity sizes used for crystal growth. In space it is possible to achieve gravitational levels ranging from $10^{-3}g_o$ to $10^{-6}g_o$. Typical cavity sizes are approximately 2 to 10 cm. From the space experiments of Radcliffe et al. (1988), density ratios $\Delta\rho/\bar{\rho}$ ranged from .7 to 10^{-6}. The highly dilute limits have been used by Roberts et al. (1987) to simulate experimentally low gravity buoyancy flows inside multiple tanks on the ground. These conditions indicate that a parametric limit of Grashof number ranging from .1 to 10^6 would cover the range of buoyancy generated flows in fluid mixing processes. The range of cases studied is shown in Table 1. Typical fluid properties such as chloroform and heptane are: $\bar{\nu} = .00495 cm^2/sec$, $\Delta\rho/\bar{\rho} = .721$, and $\tilde{D}_{ir} = 2\times10^{-5} cm^2/\text{sec}$; the properties for low density difference liquids such as water and deuterated water are: $\bar{\nu} = .00804 cm^2/sec$, $\Delta\rho/\bar{\rho} = 4.9\times10^{-6}$, and $\tilde{D}_{ir} = 2\times10^{-5} cm^2/\text{sec}$.

4.2 Characteristics of flow field evolution and interface morphology: Convective mixing

The first case is selected to give an overall picture of the phenomena. In our problem, since there is a density jump across the interface, a finite horizontal pressure gradient exists which drives the flow. Figure 2 shows the early stages of the effect of the flow field on deformation of the interface region. The kinematics of interfacial deformation is shown by contours of concentration, and the stream function contours show the flow field and its direction by velocity vector field plots. The morphology of the interface region is similar to the tilted experiments of Andrews and Spalding (1990) for short times. The flow field causes stretching and folding of the interface. A rotational flow with a strong vortex core results initially. This flow field pushes the interface region towards the top and bottom of the cavity symmetrically. Its maximum velocity is attained when the interface region has been stretched near its maximum horizontal direction ($t = 0.016$). This local maximum velocity for early times is within order of magnitude of the characteristic velocity obtained from scaling with the characteristic time T_b.

The momentum of the flow field continually stretches the interface to form an internal wave. This is shown in Figure 2b. Internal waves are known to occur in the ocean and have also been produced in several tank experiments as pointed out by

Turner (1973, pp 14-21, 48-57, 120-126). However, unlike our case these internal waves are generated experimentally by mechanical sources at the boundaries. As shown in the figure the formation of an internal wave feeds back or interacts with the flow field. This results in the formation of multiple vortices and takes place at the location of the maximum wave amplitude. This case corresponds to the formation of a stable wave. The deformation of the interface region is topologigal, it is smooth and continuous and there is no breakup. This configuration shows the point where the flow field has converted all its initial potential energy into the formation of a wave. At this point the wave dissipates all its potential energy through oscillation of the interface region.

The oscillation and decay of the internal wave with reflections at the boundaries are shown in Figure 2c. The maximum amplitude of the wave occured at about (t = .029). Subsequently the interface region behaves like a damped oscillator. Because of viscous effects and since there is no source of energy being fed into the system the oscillations decay quite rapidly. During the first cycle of oscillation from (t = .029 to .072), wall friction dissipates the energy of the wave. The equilibrium position corresponds to t=.039. Upon reflection from the boundary at t=.05 less energy is available due to dissipation. This represents the first half cycle of the oscillation. At this point the motion repeats itself, with each continual reflection at the boundary the amplitude of the wave decreases until it decays at t=.151.

The effect of the buoyancy force is to stretch and deform the interface, in this case create internal waves which decay to a stably stratified configuration. During this process a mixed region results with a certain width at the stably stratified configuration with light component fluid above the heavy component fluid. The two fluids then mix diffusively until a final state of uniform concentration field is achieved with zero potential gradients in the region. The final state which leads to uniform mixing is shown in Figure 2d. The complete stably stratified configuration occurs at t = .717. The separation of the lines represents interdiffusion from one region to another. Similar observations have also been reported in tank experiments, see Turner (1979, pp 267-270). Note that at t = 9.56 interdiffusion does not occur uniformly throughout the region. One posible explanation is that, as will be shown later, there is still flow in the stably configuration which is in the form of vortex rows. Since these vortices have variable strengths, they contibute to the spreading of the concentration field at different rates. This gives rise to unequal spreading (dispersion) rate of the concentration field. Note that at t = 23.9 the concentration lines of .1 and .9 have diffused, this process continues until the concentration lines of .4 and .6 also diffuse through the cavity. At this

point uniform mixing would have taken place. The line C=.5 would still be present, in agreement with our earlier definition of this line as a tracer, a hypothetical material line which admits diffusion through itself.

The characteristics of the flow field during various stages of mixing for the stably stratified configuration are shown in Figures 2e, 2f, 2g. At the interim to stratification the flow field with multiple vortices which was oriented vertically is now oriented horizontally (Figure 2e). The vortices are mainly concentrated near the top left hand and lower right hand walls with a weak flow field in the mixed region. This flow field is weaker than the flow field generated by the buoyancy force; it is the decay of the flow field left over from the action of the buoyancy effects and wave oscillations. It has the same order of magnitude of velocity as the viscous diffusive flow field. Thus, it represents the viscous diffusion regime. Transition from the viscous diffusion regime to mass diffusion is shown in Figure 2f. Note that in this case the vortices generated at the wall diffuse away from the wall to the core of the flow field. Regions of weak flow now occupy a much larger area. This is accompanied by an increase in the width of the mixed region. The region that is dominated by mass diffusion, where viscous diffusion has decayed, is shown in Figure 2g. In this regime the vortices that were originally generated near the wall have diffused toward the top and bottom center of the cavity. Beyond $t = 9.56$ the action of mass diffusion begins to decay. At this point the magnitude of the velocity field would approach zero as an equilibrium state is approached. Thus, the characteristics of the flow field denote three distinctive regions at the interim to mixing with various velocity scales: a buoyancy dominated region at early times which transforms to a viscous diffusive region and finally to a mass diffusive region as thermodynamic equilibrium is approached.

4.3 Effect of aspect ratio

For the above parametric value, the effect of the buoyancy force is to stretch and deform the interface into an internal wave. We now examine the effect of varying the aspect ratio on the amplitude of the wave generated. The amplitude is the vertical distance the material interface deforms from a horizontal position at midheight of the cavity. In Figure 3 we show the effect of five aspect ratios on the amplitude of the wave generated at a fixed time ($t = .029$). The aspect ratio variations correspond to varying the cavity from a square configuration (Ar = 1) to a vertical rectangle (Ar = 2 and 10) keeping the height constant, then to an horizontal rectangle (Ar = .1 and .5) decreasing the height by one tenth and one half respectively. Since the Grashof number is proportional to H^3, its magnitude would not change even though the configuration of the cavity has changed from a square to a vertical rectangle. However, note that from the

dimensionless field equations the aspect ratio plays a more dominant role in this situation. Similar to the previous case, Ar=1.23, the material interface forms a wave with a large amplitude, Ar=1. For a stable wave formation, if a vertical line is extended midlength of the cavity, the wave would be tangent to this line. We thus have a stable wave formation for the Ar=1 case. However, when the aspect ratio is increased to Ar=2 the interface deforms past this vertical line. Thus we have a situation where the material interface starts to fold on itself. Since we had decreased the width of the cavity, viscous effects are effective enough to sustain this incipient unstable wave and keep it from breaking. As the cavity is made narrower, Ar=10, the effect of the walls is to damp out wave formation. Deformations occur only near the top and bottom of the cavity. Very effective vertical shear flows develop near the interface which acts to prevent deformation of the interface at the core of the cavity. In contrast, for the horizontal configuration Ar=.5, the amplitude of the wave is very small, this is due to the fact that the potential head available to transform the material interface into a wave has decreased. In this case a smaller thickness of mixed region would result after the stratification. When the cavity approaches a horizontal slot (Ar=.1), the flow field is not effective enough to deform the interface, as we pointed out earlier; in this case the one-dimensional diffusive limit of mixing is approached.

4.4 Effect of Grashof number

The dependence of both Ar and Gr on height prevents independent variation of these parameters. However, if the aspect ratio is fixed (Ar = 1), one may vary either the properties of the fluids or the ratio of the gravitational field to investigate the effect of Gr. In Figure 4, we show the effect of Gr on interface morphology. Unlike the previous cases we consider the lower values of Gr to investigate the other end of the spectrum. These values represent conditions that can only be obtained under microgravity environment. The resulting deformation of the interface for Gr of order 10^3 is similar to the previous case in Figure 3, in spite of the change in aspect ratio. As the Grashof number decreases there is less potential energy head available to deform the interface. The case for Gr = 3.73 corresponds to the situation where the characteristic flow field velocity is of the order of the diffusive velocity. In this case the interface does not stretch and one-dimensional diffusion occurs for mixing. Thus, the effect of increasing the Grashof number is to stretch and fold the interface region. The amount of stretching and folding depends on its magnitude.

4.5 Internal breaking wave

The aspect ratio studies gave us a first glimpse into nonlinear wave formation. We now study this phenomena in more detail. In Figures 5a,b,c, we show a case

where the Grashof number is increased one order of magnitude, $Gr = 3.73\times10^5$. This leads to the formation of a wave which folds on itself, similar to break waves in the ocean, Figure 5a. Unlike the previous case for Ar=2, this wave is unstable and it soon breaks at $t = .012$, Figure 5b. What makes this phenomenon interesting is that it is an internal wave. Such phenomenon of internal breaking waves has been discussed by Turner (1973, pp 120-123) and has also been observed by McEwan (1983a,b) through experiments to study the details of wave breaking inside tanks. In contrast to the formation of a wave for Gr up to 10^4 which oscillate before a stably stratified configuration is reached, in this case the material interface continually stretches and deforms until it breaks, no oscillation occurs. The breaking of the wave gives rise to an increased number of vortices in the flow field. These vortices serve as stirring mechanisms to homogenize the mixing region. This leads to a much thicker stratified mixed region than the previous cases. Upon stratification the flow field is transformed from multiple vortices to a single vortex in the core, Figure 5c. For longer time, the stratification leading to complete mixing is similar to the previous case examined ($Gr = 1.45\times10^4$), in that vortex rows develop in the flow field as thermodynamic equilibrium is approached. Note also that droplet formation occurs near the top and bottom walls; they grow and break-off similar to droplet formation in R-T instability. The break-off occurs at the neck of the drop. Droplet reattachment occurs before final stratification.

4.6 Chaotic mixing

A horseshoe map involves continuous deformation of a material region (a blob or a square) by a flow field which stretches and folds the region on itself, Ottino (1979, chps 5 & 7). One of the necessary conditions for a system to display chaos is that the flow field produces horseshoe maps. As discussed by, Chien, Rising, and Ottino (1986), the presence of a horseshoe function in a mixing system involves superposition of forward and backward transformation with the initial location of the material region. In our case this requires careful examination of the time sequence evolution of the interface region of the two fluids in Figure 5. When breakup occurs, there is no periodicity in the flow field to allow superposition of striation patterns prior to breakup. Even though the structure is similar to that of a hoseshoe map, it is difficult to ascertain the presence of a horseshoe function with any degree of certainty. However, another measure, as will be shown, such as the length of stretch of the interface indicates exponential growth in this parametric region. This behaviour is known to occur in chaotic regions of mixing. Chaotic mixing is effective for fluid mixing. This is verified in our results, for a much shorter length of time, a much wider mixed region resulted.

4.7 Diffusive Mixing

Of great importance to materials processing is the region where diffusive mixing occurs and the material interface remains undistorted while mixing takes place uniformly. This case is particularly useful to crystal growers because deformation of solute fields during crystal growth leads to unwanted segregation effects, see Chang and Brown (1983). These situations adversely effect crystal quality because of inhomogeneity of the solute field. In Figure 6, we show the case which leads to diffusive mixing without distortion of the interface. In this case a weak rotational flow field results, and the characteristic velocity is of the order of the mass diffusive velocity. Buoyancy forces are smaller than viscous forces, the flow field has minuscule effect on the concentration field and it stays constant for the time considered. In this case, by virtue of the low value of $Gr = .37$, the one-dimensional limit is approached as we had speculated earlier.

The fact that mass transport can be induced by both convection and diffusion was pointed out by Maxwell (1860). This also suggests that for miscible systems, diffusion and convection always occur together, even if the system is isothermal or isobaric. This fact seperates mass diffusion that occurs in fluids from heat diffusion that occurs in solids. Even though convection is very small for the case shown, mass transport still occurs, and diffusion is the dominant mechanism. This limiting case can serve to illustrate that even when convection is negligibly small, diffusion generates its own convection. The case for vanishingly small convective field has been used in many textbooks for the solution of diffusion problems, see for example Cussler (1984, pp 55-85) and Crank (1986, pp 1-10). The computational results can be used to compare to the closed form solution obtained with the assumption that the nonlinear convective terms are negligible. In this case, there is a decoupling of the vorticity field from the concentration field. This leads to the simple approximate problem:

$$\frac{\partial C}{\partial t} = \frac{1}{Sc}\left[Ar^2\frac{\partial^2 C}{\partial x^2} + \frac{\partial^2 C}{\partial y^2}\right]$$

$$\nabla C^* \cdot \vec{n} = 0 \quad \text{on} \quad \Gamma.$$

We obtain the closed form solution

$$C(x,y,t) = \left\{\frac{1}{2} + \frac{2}{\pi}\sum_{l=0}^{\infty}\frac{(-1)^l}{(2l+1)}\cos(2l+1)\pi x \cdot \exp - \left[(2l+1)^2\pi^2(Ar^2/Sc)\ t\right]\right\}.$$

The simplification has great significance, it implies that even if we have a three dimensional cavity the solution is still one-dimensional. Note that in dimensional units the

group $(Ar^2/Sc)\ t$ reduces to $(\bar{D}_{ir}/L^2)\ t^*$, which is the expected proper form of the solution. The proper characteristic time T_D is also recovered. Comparison of the one-dimensional closed form solution to the results in Figure 6 is shown in Figure 7. The close agreement shows that the classical solutions for diffusion problems give excellent results when convection is vanishingly small. For experimenters who use microgravity for materials processing phenomena, it shows that good control of convective flow fields can be achieved in a space laboratory.

4.8 Comparison of local velocity scales to the computational results

Two types of scaling occur, local and global time scaling. The global scaling provides an overall scaling of the phenomena. The local scaling takes into account the local events influencing the process and can yield approximate magnitude of the flow field. In Table 2 we show the characteristic local velocity predicted from the characteristic local time (see Table 3) for various Gr numbers. The local velocity is scaled using the height of the cavity as characteristic length with the proper characteristic time. V_{mag} indicates the magnitude of the velocity field from the computational results at the appropriate local characteristic time. The results show that when the proper characteristic time is used reasonable agreement is obtained in comparison with the computational predictions. This shows the importance of local scaling for obtaining the proper characteristic velocity in this class of problem.

4.9 Descriptors to quantify mixing

We use three descriptors to quantify mixing for flows driven by buoyancy forces, namely: the local mixing efficiency, the interface width W of the mixed region and its elongation length L as a function of time. The dimensionless width and length are defined as, $W = (W^* - W_o)/W_o$ and $L = (L^* - L_o)/L_o$, where subscript o denotes the initial value at time zero. The width of the interface is taken as the average distance between the maximum and miximum concentration contour. In Figures 8, 9, and 10 we show the width of the interface region as a function of time.

4.9.1 Variation of interface width

For the nominal value of Gr of order 10^4 which brackets the diffusive mixing (Gr of order 1) and chaotic mixing (Gr of order 10^5) regime as shown in Figure 8, three distinct mixing regions occur: the convective region which results in wave formation, the oscillatory region, and the diffusive region. In the convective region the width of the interface expands and contracts. This occurs at the very early stages of the flow development. This is also in agreement with the experimental findings of Andrews and Spalding (1990) for their tilt experiments. Further contraction and expansion continue

through the oscillatory region until a stable stratification results. In the oscillatory region Kelvin-Helmholtz instability through horizontal shear results in the contraction and expansion of the interface region. The final stage of diffusive mixing is accompanied with the decay of the flow field and shows an exponential like behaviour toward homogeneous mixing. This exponential like behaviour is due unequal spreading of the concentarion field in the stably stratified configuration.

The other cases of diffusive and chaotic mixing are shown in Figures 9 and 10. The purely diffusive regime exhibits the same character as the late stages of the convective mixing which is to be expected since mixing is one-dimensional in both cases. In comparison to Figure 8, it takes more time for the fluid to diffuse through equivalent widths as compared to the convective regime. This is due to the existence of a weak flow field which does not deform the interface. In contrast, the chaotic regime provides very effective mixing. For the same dimensionless time, the width of the interface increases 3 times as much in comparison to the convective mixing case and to about 7 times greater than the diffusive mixing case.

4.9.2 Elongation of the material interface

Another measure to quantify mixing is the elongation of the material interface due to the flow field. The basic three cases of convective, diffusive, and chaotic regimes are shown in Figures 11, and 12. In the convective regime, the effect of the flow field is to transform the initially vertical material interface to an horizontal position. In the early stages of flow development the material interface continually elongates until a maximum is reached. This maximum corresponds to the internal wave formation region. The material interface decreases in length in the oscillatory region to conform to the horizontal width of the cavity. Although the length of the material interface decreased, the width of the mixing region increases which is a better indicator of the degree of mixing for this region. Contraction and expansion of the length of the material interface also occur. The plumes at the top and bottom walls eventually decay until a stable stratification is reached. In the stably stratified configuration, since the length of the material interface remains constant, it is no longer a good indicator of mixing. However, the width W of the mixing region continues to grow, and serves as a better indicator of mixing, until equilibrium is achieved. Note that the intial and final lengths are not equal, this is because $Ar \neq 1$.

The diffusive and chaotic mixing regimes are shown in Figure 12. As expected, in the diffusive regime the length of the material interface remains constant. Whereas in the chaotic mixing regime the length increases exponentially. In this case, the flow field is very effective at stretching the material interface to its maximum length.

Because of internal wavebreaking, there is no oscillatory mode for this case. Instead there is an abrupt transition to a stratified configuration. When turbulence from wavebreaking dissipates, complete mixing occurs via the diffusive mode. Note for the same time interval the flow field stretches the interface 3 times as much as the convective case. And the maximum length occurs for 1/4 the time as that of convective mixing. Thus, the effect of the flow field is to stretch the material interface until a maximum is reached. The maximum length of stretch determines the width of the mixing region once stratification is achieved. If the flow field is weak, diffusive mixing occurs without stretching the interface.

4.9.3 Local mixing efficiency

Laboratory experiments to quantify stratified mixing through internal wavebreaking have been carried out by McEwan (1983a,b). The qualitative features of internal mixing by breaking such as density microstructures, regions of density instability, and interleaving are shown to occur experimentally. A simple method to calculate mixing efficiency based on a particle exchange model shows that for a linear stratification the mixing efficiency η is on the order of 1/4 (McEwan 1983a). However, in defining mixing efficiency as the ratio of potential energy from stratification to kinetic energy gained through shear, a major component of the overall energy which does not contribute to mixing is from viscous dissipation. In McEwan (1983b), careful experiments were designed to account for viscous dissipation, final results show that the assumption of similarity between buoyancy and mass transfer used by previous investigators are valid. The efficiency values calculated in (1983b) agree closely with the particle exchange model in (1983a). Comparison with our model suggests that we can use a similar method to calculate mixing efficiency. The internal wave generated is based on the potential head available ($E = \Delta\rho\, n g_o\, H$). Based on the total potential head, the internal wave may or may not break. This potential head results in certain wave formation that has a certain potential energy which is dependent on peak to peak amplitude ($P = \Delta\rho\, n g_o (y^{*f} - y^{*i})$. (The peak to peak amplitude is denoted by $(y^{*f} - y^{*i})$.) This energy is dissipated either through internal oscillation or wavebreaking, which gives rise to a certain stratification thickness (δ). The efficiency may be approximated as $\eta = \delta / (y_f - y_i)$. For the three cases examined, convective, chaotic, and diffusive, we obtain mixing efficiencies of .26, .34, and 0.0 respectively. The convective case agrees quite well with the predicted value of 1/4 , since in the chaotic case, breaking occurs we would expect η to increase, however, its magnitude is within the limits of the cases reported in McEwan (1983b). Finally a zero mixing efficiency results for diffusive mixing since volume elements never exchange position and the system gains no

potential energy, this is in agreement with the definition in McEwan (1983a).

4.10 Comparison of the features of our model problem to Rayleigh-Taylor characteristics

An analog to our model problem is the classical Rayleigh-Taylor instability of superposed fluids with the heavier component overlying the lighter component, see Chandrasekhar (1961). It is well known that short wavelength instabilies give rise to growth of the interface between two fluids. Daly (1967, 1968) has shown computationally the evolution of the interface inside a bounded cavity. His results show that in the late stages of the Rayleigh-Taylor (R-T) instability, Kelvin-Helmholtz (K-H) instability give rise to waves at the interface. These waves form near the neck of the spike. With the inclusion of surface tension, Daly (1969) has shown the conditions leading to drop formation in agreement with the experimental findings of Melcher and Hurwitz (1967). Our model problem exhibits many of the features that occur in the classical R-T instability problem. Because of the magnitude of Gr number the nonlinearity is very important except for the limiting case of small or $Gr \rightarrow 0$. This is in contrast to the linear stability problem of R-T where nonlinearity is neglected. Unlike the classical R-T where the density jump is parallel to the body force; in our model problem the density jump is perpendicular to the body force, as a result flow is initiated without having to introduce a perturbation. The small scale features at the interface due to the growth of small wavelength perturbation, as shown experimentally by Andrews and Spalding (A&S) (1990) for the no tilt case, do not occur in our results. However, the numerical simulations of Youngs (1984), show that these small features occur for the multiple wavelength initial perturbation cases. Even though our model problem corresponds to a much larger tilt angle in comparison to the cases considered by A&S, the basic character of the flow field dominated by an overturning two dimensional motion still occurs.

The late stages of convective mixing for our case show similar behaviour to the late stages of R-T instability. One of the features of R-T is the lateral growth K-H instability in the nonlinear regime. In our case, oscillation of the wave causes growth of K-H instability due to the shear components of the velocity field. This is manifested by the undulatory features of the interface region. A feature, usually uncommon in classical R-T, is the evolution of plumes at the top and bottom corners of the cavity. This is shown to occur for the slightly tilted experiments of A&S. In the case of A&S, these wall plumes are attributed to the short wavelength instabilities due to the half sawtooth initial perturbation. A similar behaviour occurs for our case. Because vorticity is generated at the walls, a slow dragging effect of the plumes near the walls occurs before final stratification is achieved.

The features of interface breakup and droplet formation also occur for the chaotic mixing case. Droplet formation occurs near the top and bottom of the cavity as shown in Figure 5b. The growth of the droplet is similar to the spike formed during R-T instability which is usually shown to occur as a single event (Daly, 1969). However, in our case multiple events occur simultaneously with the droplet formation. This includes the breakup of the interface region, and multiple droplet formation. As shown in Figure 5b the frontal area of the droplet increases in size while the neck gets thinner. This results in the seperation of the drop from the source region. The breakup occurs right at the neck in the thinner region. Note that reattachment of the droplets occurs before a stably stratified configuration is achieved.

4.11 Phenomenological discussion and related experiments

According to Youngs (1984), the quadratic law for the growth rate of the mixed region of the interface (i.e. $W^* = 2\alpha \cdot At \cdot g\, t^{*2}$, $\alpha = .04$) by R-T instability is valid only for short wavelength initial perturbation. The experiments of Read (1984) show quite clearly the validity of the quadratic law for a number of experimental cases of mixing inside tanks by R-T instability. However, for large amplitude long wavelength initial perturbation, the quadratic law ceases to be valid. The growth rate corresponding to the most unstable wavelength, see Chandrasekhar (1961), for viscous fluids is given by:

$$n_m = \left\{ \pi \frac{n g_o}{\lambda_m} At \right\}^{1/2} \quad \text{and} \quad \lambda_m = 4\pi \left\{ \frac{\bar{\nu}^2}{n g_o} \quad \frac{1}{At} \right\}^{1/3} .$$

Based on the trends of the physics, When $Gr \to 0$ the R-T problem (if mass diffusion is considered) and our model become equivalent, that is they have the same solution. In Table 3 we show the corresponding wavelength and growth rate for various Gr numbers. According to linear theory of stability as the level of gravitational acceleration ng_o decreases, λ_m increases and the growth rate decreases. In comparison to the height of the cavity H, λ_m is much greater. This implies that a situation that is unstable on earth can become stable in space if ng_o can be reduced to sufficiently small values. In this case the diffusive limit would be approached as we had shown. And the closed form solution is applicable to both R-T and our model problem. Note also that the characteristic time n_m^{-1} of the growth rate of the perturbation is within the same order of magnitude as predicted by the buoyancy time scale T_b. However, as expected when the Gr number increases and nonlinearity becomes important, the disparity between T_b and n_m^{-1} increases.

Based on the comments of Sharp (1984) the phenomenology of R-T instability occurs in 4 basic stages: (1) the linear evolution of the interface due to small

amplitude perturbation, (2) the nonlinear growth of these perturbations of the order of the wavelength, (3) the development of the interface structure into spikes and bubbles, and (4) the breakup of the spike by various mechanisms leading to turbulent or chaotic mixing. These phenomenology are similar to the features exhibited in our model problem for high Gr numbers with the exception of stages (1) and (2).

An alternate viewpoint for the interpretation of our results is based on the concept of passive and active interfaces by Aref and Tryggvason (1984). The characteristics of the observed structures of our interfaces may be quantified in those terms depending of the magnitude of Gr number. As we have shown depending on the magnitude of Gr, three distinct flow field regimes occur: convective, diffusive, and chaotic. These flow field regimes are characterized based on the morphological patterns displayed by the interface region when it is advected by the flow field. The diffusive regime displays a "passive" interface. The convective regime shows the "weak coupling limit" where the flow field is slightly influenced by the interface structure. This occurs during the transition of the interface to the stratified configuration. The oscillation of the interface acts as a "feed back" to the flow field. In this case, the interface structures of "whorls" and "tendrils" as described by Berry et al. (1979) and Ottino (1989) are also exhibited. For the convective regime, the evolution of the interface into a wave may be interpreted as a whorl resulting from the rotation of the flow and its subsequent oscillation has the characteristic of tendrils, note the secondary waves on the interface region (Figure 2c). However, in the chaotic limit, the interface may be seen as passive only for a very short time; it soon displays the characteristic of an active interface with features such as spikes, bubbles, and breakup similar to the late stages of R-T.

The limiting cases of diffusive and chaotic mixing have applications to materials processing. Some delicate processes require purely the diffusive regime such as crystal growth, while others require efficient mixing before a process can be carried out. This occurs in the growth of crystals with binary components where a solute field of low concentration exist. Sometimes it is necessary to have a homogeneous liquid phase before the process is carried out. The range of cases studied give insight into what can be accomplished with buoyancy generated flow fields under steady microgravity conditions. And these cases can serve as a guideline to what can be achieved in space.

5. Concluding remarks

We investigated a model problem to study fluid mixing due to buoyancy generated flows with emphasis on microgravity conditions. Three distinctive mixing regimes are identified for a range of Grashof numbers: diffusive, convective, and

chaotic. In the diffusive regime Gr of order 1 or less, mixing occurs without stretching the interface region. The interface spreads out uniformly as mixing occurs and the characteristic velocity approaches the diffusive limit. This case compares well with the one-dimensional closed form solution of classical diffusion problems. It shows quite clearly the conditions under which the classical solution holds. Whereas in the convective regime, Gr of order between 10 to 10^4, events leading to stratification occur with various important differences. In the region for Gr between 10 and less than 10^3, very gentle overturning motions occur without internal wave formation. However, for Gr number on the order of 10^3 to 10^4, the overturning motion stretches and folds the interface region which leads to formation of an internal wave with various amplitudes. These waves oscillate, and the decay of oscillation leads to a stably stratified configuration. Wave generation enhances mixing by dissipating energy at the interface region, this leads to an increase in the width of the mixed region. Finally, in the chaotic regime, Gr number on the order of 10^5 or greater, continuous stretching and folding of the interface occur until it breaks. No oscillation of the resulting wave formation takes place. This wave exhibits the characteristics of internal breaking waves. Once the wave breaks, a very large mixing width region results. Thus, the chaotic regime is very effective for mixing. Independent of the convective and chaotic regime, when stratification takes place, final uniform mixing occurs via mass diffusion.

Each mixing regime has its own characteristic flow field. The mixing efficiency is greatly dependent on the type of flow field. The flow field gives rise to two basic structures, namely, tendrils and whorls. In the convective regime both whorls and tendrils occur. The whorl occurs at the beginning of the flow, and this results in the formation of the wave. When this wave oscillates, a tendril structure occurs. During the wave formation, the flow field transforms from single to multiple vortices (cells). The decay of wave oscillation leads to stable stratification of the two fluids. This period is marked by the decay of buoyancy forces. At this point the flow field changes from vertical to horizontal stacks of vortices. These vortices are generated by wall effects during the viscous diffusion period. For the long time scale, mass diffusive period, the vortices diffuse from the wall to the flow field. The flow field slowly decays until the fluids are uniformly mixed.

In the diffusive regime, a steady flow results. Steady flows are known to be less effective in producing mixing. This is quite evident in the diffusive regime, since the length of the material interface remains constant while mixing occurs. On the other hand, chaotic mixing is very efficient for mixing. This is evident by the stretching, which increases exponentially, and folding of the interface region. The flow field is

unsteady, and large number of vortices are generated. These vortices serve as stirring mechanisms to produce a stratified mixed region.

We examined the implications of both local and global time scales. Three local time scales occur during mixing generated by buoyancy forces. A time scale to denote the decay of buoyancy effects (T_b), a viscous diffusion time (T_v), and a mass diffusion time (T_D). The global time scale depends on the magnitude of the Gr number, and for a particular Gr number, scaling with the appropriate local time scale yields approximate results for the characteristic local velocity. The local time scale depends on the events occuring during the mixing process. These events can be summarized as follow : (1) an overturning motion which may lead to internal wave formation (T_b), (2) stable stratification which follows from oscillations or wavebreaking (T_v), and (3) lastly diffusive mixing which takes place until thermodynamic equilibrium is reached or no concentration gradient exists in the flow field (T_D). Scaling with the appropriate local time scale yields the approximate magnitude of the local velocity. Note that for the limiting cases of $Gr \to 0$ or $Gr \to \infty$, there is only one appropriate local time scale, T_D or T_b respectively. For these cases the phenomena are dependent on a single time scale, whereas multiple time scales occur for the cases that lie between the limiting cases. The appropriate global time scale, based on the magnitude of Gr, is summarized as follows: for $Gr \to 0 \quad T = T_D$, $10 \le Gr \le 1\times10^6 \quad T = T_v$, and $Gr > 10^6 \quad T = T_b$. However, with the inclusion of the limiting case $Gr \to 0$, we found that for our parametric range even when we scaled with T_v the proper characteristic time T_D is recovered.

Descriptors to quantify mixing such as width of the mixed zone, elongation of the interface, and local mixing efficiency have shown the characteristics of mixing generated by buoyancy forces. For high Gr numbers where nonlinearity is important the width of the mixed region for the convective and chaotic regime contracts and expands as time increases, until the stably stratified configuration is reached. In the stratified configuration, the mixed region increases steadily in time until equilibrium is achieved. Similar trends occur for the diffusive regime of mixing. The elongation of the interface for the chaotic and convective regime increases exponentially with time. However, in the convective regime, the oscillation region provides partial restoration of the flow. Whereas, in the chaotic regime, no oscillation occurs, the length decays as t^{-1}. In the diffusive limit the length of the interface is independent of time. The local mixing efficiencies for the convective, chaotic, and diffusive regimes are respectively .26, .34, and 0. These values are in agreement with typical values reported by McEwan. Comparison of our results with the linear theory of stability shows that for low Gr numbers

the characteristic time for growth rate of a perturbation is in good agreement with the time predicted by the buoyancy frequency. The local characteristic velocity scales show reasonable approximate correlation with computational values.

From the point of view of crystal growers, the results for Gr=.37 are encouraging. Because the space environment offers the potential to achieve low gravitational levels, the results indicate that there exist parametric regions where the diffusive regimes can be obtained. Attaining the diffusive regime is basically the region of interest for the crystal growers. This means that it is possible to obtain a solute field which diffuses uniformly. This is very important to many crystal growth phenomena where nonuniform distribution of the solute field can cause unwanted segregation effects. These effects degrade crystal quality. Thus, microgravity environment provides a unique setting where delicate materials processing can be controlled. This opens the door to many other new phenomenological investigations.

6. Acknowledgement

The support of NASA's Code SN Microgravity and Applications Division is gratefully acknowledged.

7. References

Andrews, M.J.; and Spalding, D.B.: A Simple Experiment to Investigate Two-Dimensional Mixing by Rayleigh-Taylor Instability. Phys. Fluids A, vol. 2, no. 6, 1990, pp. 922-924.

Aref, H.; and Tryggvason, G.: Vortex Dynamics of Passive and Active Interfaces. Physica, vol. 12D, 1984, pp. 59-70.

Berry, M.V.; et al.: Quantum Maps. Ann. Phys., vol. 122, 1979, pp. 26-63.

Book, D.L.: Finite-Difference Technique for Vectorized Fluid Dynamics Calculations. Springer-Verlag, New York, 1981.

Boris, J.P.; and Book, D.L.: Flux-Corrected Transport I: SHASTA—A Fluid Transport Algorithm that Works. J. Comput. Phys., vol. 11, 1973, pp. 38-69.

Chandrasekhar, S.: Hydrodynamic and Hydromagnetic Stability. Oxford University Press, Oxford, UK, 1961.

Chang, J.C.; and Brown, R.A.: Radial Segregation Induced by Natural Convection and Melt/Solid Interface Shape in the Vertical Bridgman Growth. J. Cryst. Growth, vol. 63, 1983, pp. 343-364.

Chien, W.L.; Rising, H.; and Ottino, J.M.: Laminar Mixing and Chaotic Mixing in Several Cavity Flows. J. Fluid Mech., vol. 170, 1986, pp. 355-377.

Crank, J.: The Mathematics of Diffusion. Oxford University Press, Oxford, UK, 1986.

Cussler, E.L.: Diffusion, Mass Transfer in Fluid Systems. Cambridge University Press, New York, 1984.

Daly, B.J.: Numerical Study of Two Fluid Rayleigh-Taylor Instability. Phys. Fluids, vol. 10, no. 2, 1967, pp. 297-307.

Daly, B.J.: 1969, Numerical Study of the Effect of Surface Tension on Interface Instability. Phys. Fluids, vol. 12, no. 7, 1969, pp. 1340-1354.

Duval, W.M.B.; and Jacqmin, D.A.: Interfacial Dynamics of Two Liquids Under an Oscillating Gravitational Field. AIAA J., vol. 28, no. 11, 1990, pp. 1933-1941.

Duval, W.M.B.: The Kinematics of Buoyancy Induced Mixing. To be published in the Proceedings of the Eighth European Symposium on Materials and Fluid

Sciences in Microgravity, Universite Libre de Bruxelles, Begium, 12-16 April, 1992.

Frohberg, G.; Kraatz, K.H.; and Wever, H.: Diffusion and Transport Phenomena in Liquids Under Microgravity. Proceedings of the Sixth European Symposium on Materials Science Under Microgravity Conditions, ESA SP-256, W.R. Burke, ed., 1986, pp. 585-591.

Galster, G.; and Neilsen, K.F.: Crystal Growth From Solution—Spacelab. Proceedings of the Fifth European Symposium on Materials Sciences under Microgravity, ESA SP-222, T.G. Duc and T.T. Hunt, eds., 1984, pp. 189-191.

Gerbi, D.J.; et al.: Growth of Organic Crystals in a Microgravity Environment. J. Cryst. Growth, vol. 76, 1986, pp. 673-680.

Maxwell, J.C.: On the Motions and Collisions of Perfectly Elastic Spheres—Part 1. Phylos. Mag., vol. 19, 1860, pp. 19-32.

Maxwell, J.C.: On the Process of Diffusion of Two or More Kinds of Moving Particles Among One Another—Part 2. Phylos. Mag., vol. 19, 1860, pp. 21-37.

McEwan, A.D.: The Kinematics of Stratified Mixing Through Internal Wavebreaking. J. Fluid Mech., vol. 128, 1983, pp. 47-57.

McEwan, A.D.: Internal Mixing in Stratified Fluids. J. Fluid Mech., vol. 128, 1983, pp. 59-80.

Melcher, J.R.; and Hurwitz, M.: Gradient Stabilization of Electrohydrodynamically Oriented Liquids. J. Spacecr. Rockets, vol. 4, 1967, pp. 864-871.

Nagata, S.: Mixing Principles and Applications. Halsted Press, New York, 1975.

Ottino, J.M.: Description of Mixing with Diffusion and Reaction in Terms of the Concept of Material Surfaces. J. Fluid Mech., vol. 114, 1982, pp. 83-103.

Ottino, J.M.: The Kinematics of Mixing: Stretching, Chaos, and Transport. Cambridge University Press, New York, 1989.

Ottino, J.M.; Ranz, W.E.; and Macosko, C.W.: A Lamellar Model for Analysis of Liquid-Liquid Mixing. Chem. Eng. Sci., vol. 34, 1979, pp. 877-890.

Ottino, J.M.; Ranz, W.E.; and Macosko, C.W.: A Framework for Description of Mechanical Mixing of Fluids, AIChE J., vol. 27, no. 4, 1981, pp. 565-577.

Ottino, J.M.: Description of Mixing With Diffusion and Reaction in Terms of the Concept of Material Surfaces, J. Fluid Mech., vol. 114, 1982, pp. 83-103.

Radcliffe, M.D.; et al.: Organic Crystals in Low Earth Orbit. J. Cryst. Growth, vol. 92, 1988, pp. 581-590.

Read, K.I.: Experimental Investigations of Turbulent Mixing by Rayleigh-Taylor Instability. Physica, vol. 12D, 1984, pp. 45-58.

Roache, P.J.: Computational Fluid Dynamics, Hermosa, Alburquerque, NM, 1972.

Roberts, G.D.; et al.: Simulation of Fluid Flows During Growth of Organic Crystals in Microgravity. NASA TM-88921, 1987.

Sharp, D.H.: An Overview of Rayleigh-Taylor Instability. Physica, vol. 12D, 1984, pp. 3-18.

Turner, J.S.: Buoyancy Effects in Fluids. Cambridge University Press, Cambridge, MA, 1973.

Uhl, V.W.; and Gray, J.B.: Mixing Theory and Practice. Academic Press, New York, 1966.

Youngs, D.L.: Numerical Simulation of Turbulent Mixing by Rayleigh-Taylor Instability. Physica, vol. 12D, 1984, pp. 32-44.

List of Tables

Table 1 Parametric range for buoyancy generated flows.

Case	Figure	Ar	*Gr*	*Sc*
1	2	1.3	1.45×10^{4}	402
2	3	1	7.43×10^{4}	402
3	3	2	7.43×10^{4}	402
4	3	10	7.43×10^{4}	402
5	3	.5	9.29×10^{3}	402
6	3	.1	74.3	402
7	4	1	3.73	247
8	4	1	3.73×10^{1}	247
9	4	1	3.73×10^{2}	247
10	4	1	3.73×10^{3}	247
11	5	1	3.73×10^{5}	247
12	6	1	.37	247

Table 2 Comparison of local velocity scales to computational results.

Gr	$V_b(cm/s)$	$V_v(cm/s)$	$V_D(cm/s)$	$V_{bmag}(cm/s)$	$V_{v_{mag}}(cm/s)$	$V_{Dmag}(cm/s)$
0	0	-	-	-	-	-
.37	4.26×10^{-4}	9.87×10^{-4}	4.0×10^{-6}	-	-	2.1×10^{-6}
1.5×10^{4}	.118	.0014	3.44×10^{-6}	.086	.0008	3.0×10^{-6}
3.73×10^{5}	.427	9.87×10^{-4}	4.0×10^{-6}	.34	2.4×10^{-4}	-
∞	∞	-	-	-	-	-

Table 3 Comparison of length and time scales to linear stability theory.

Gr	$T_b(s)$	$T_v(s)$	$T_D(s)$	$\lambda_m(cm)$	H (cm)	$n_m(s)^{-1}$	$n_m{}^{-1}(s)$
0	∞	-	-	∞	-	0	∞
.37	1.17×10^{4}	5065	1.25×10^{6}	109	5	3.23×10^{-5}	3.04×10^{4}
1.5×10^{4}	49.1	4184	1.68×10^{6}	3.76	5.8	4.48×10^{-2}	22.3
3.73×10^{5}	11.7	5065	1.25×10^{6}	1.10	5	3.21×10^{-1}	3.1
3.73×10^{9}	.117	5065	1.25×10^{6}	.05	5	1.51×10^{2}	6.62×10^{-3}
∞	0	-	-	0	-	∞	0

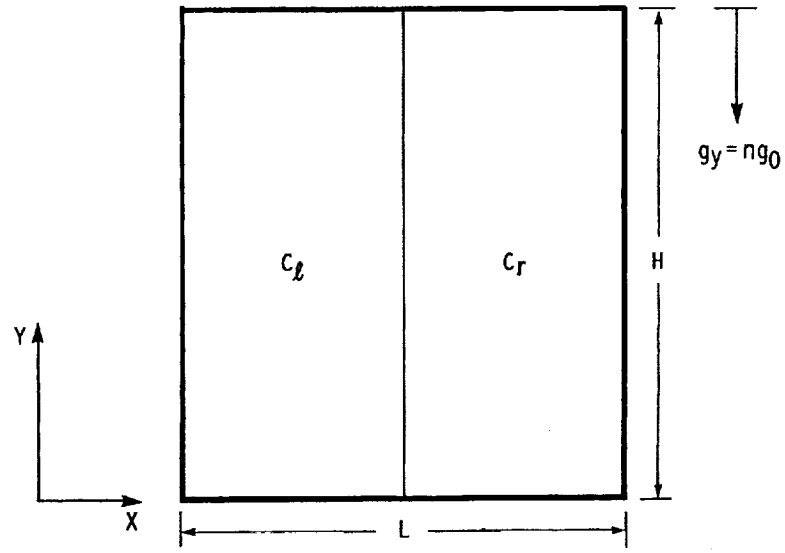

Figure 1.—Physical description of two fluids in contact at an interface.

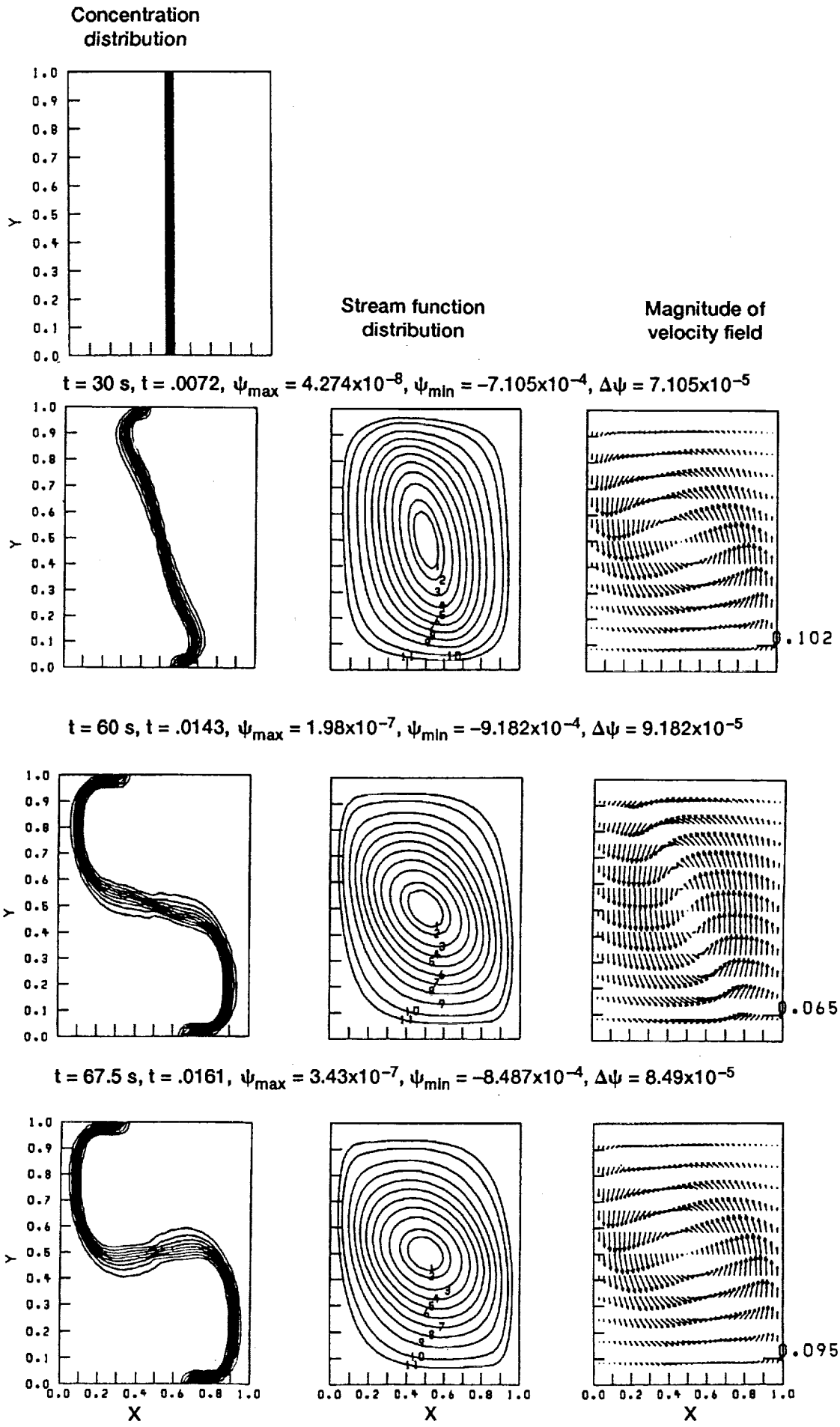

Figure 2(a).—Initial deformation of a material interface Gr = 1.45×10^{4}, Ar = 1.3, and Sc = 402.

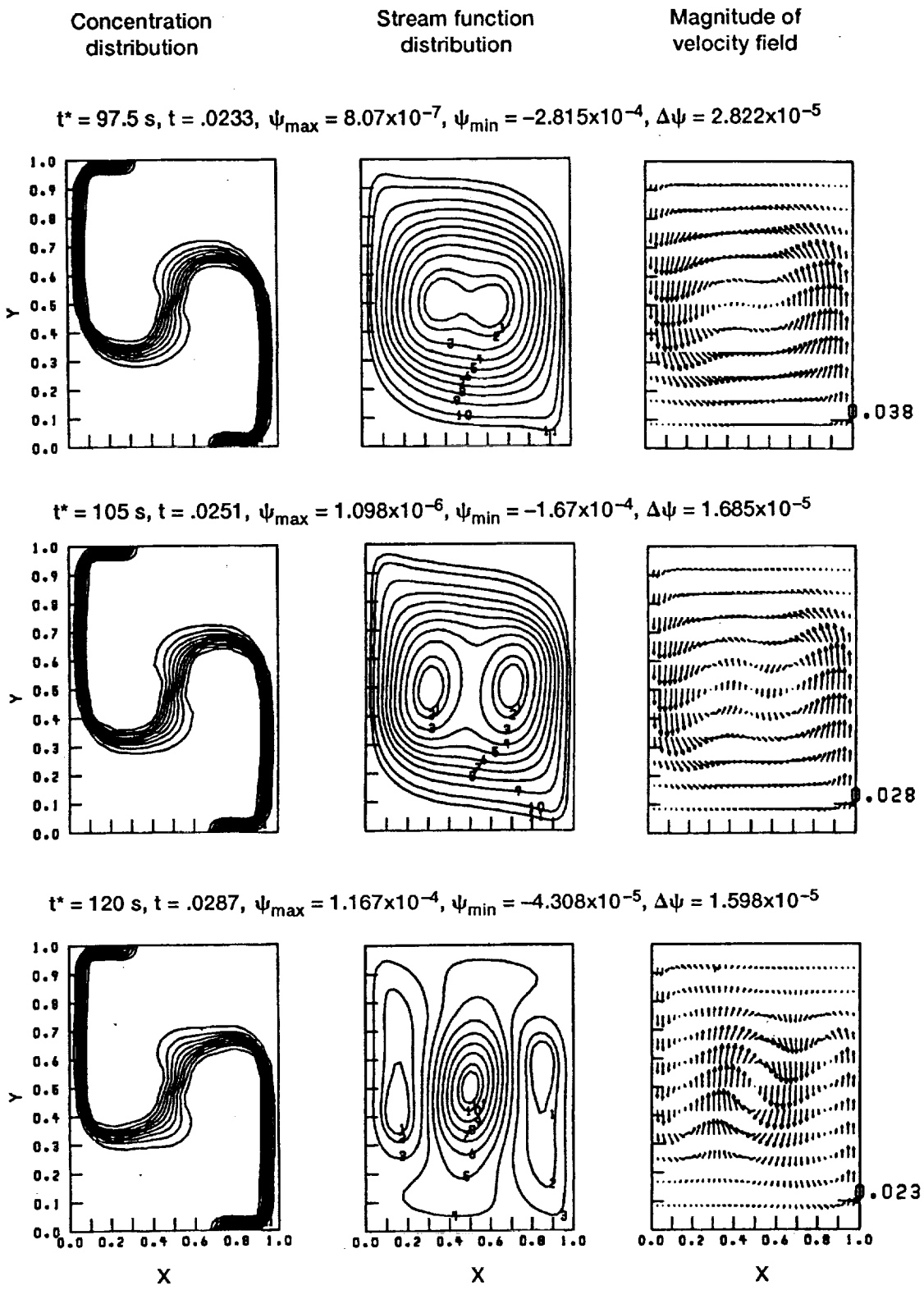

Figure 2(b).—Transformation of a deformed interface into a stable internal wave.

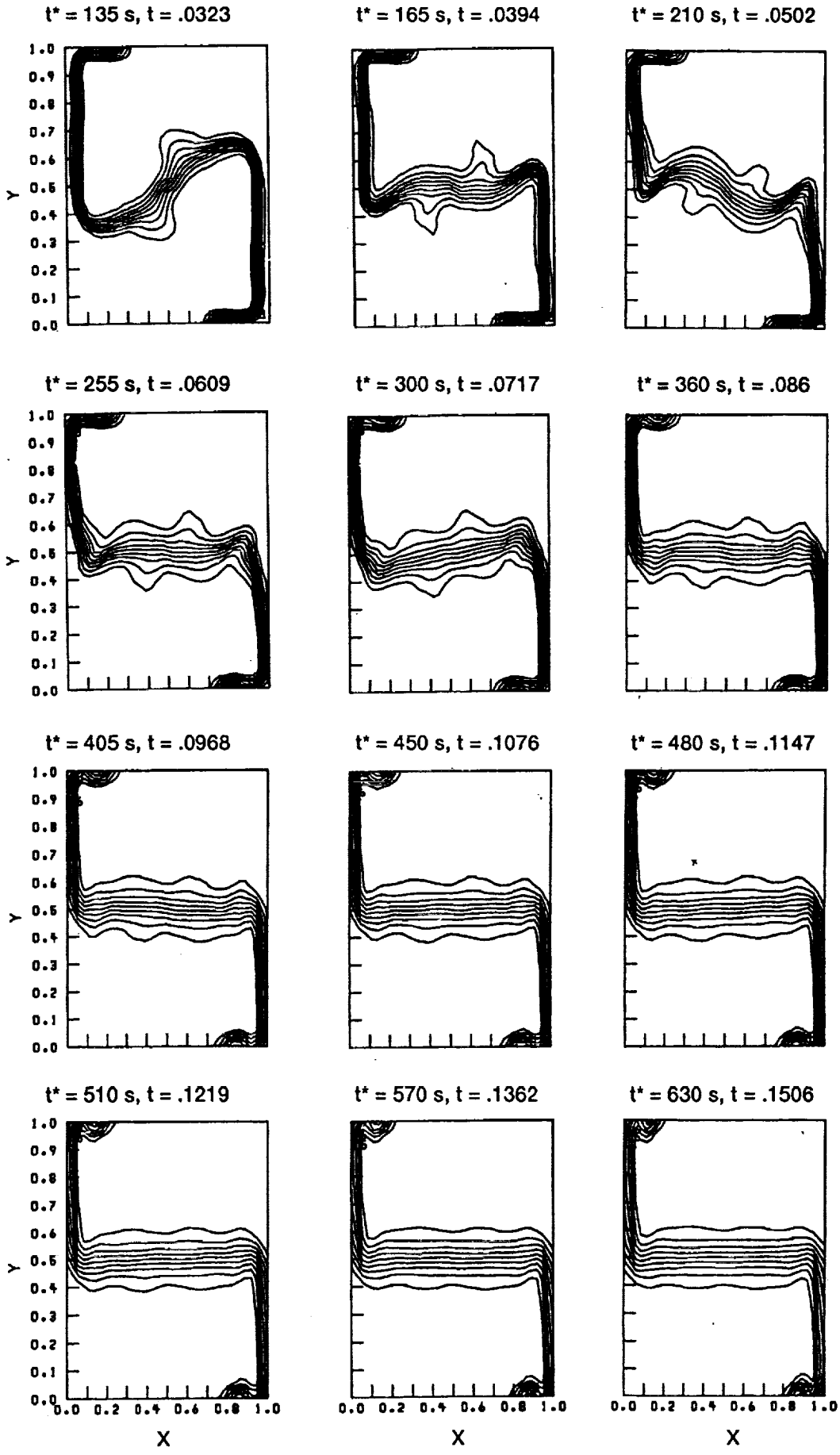

Figure 2(c).—Oscillation and decary of an internal wave with reflections at the boundaries.

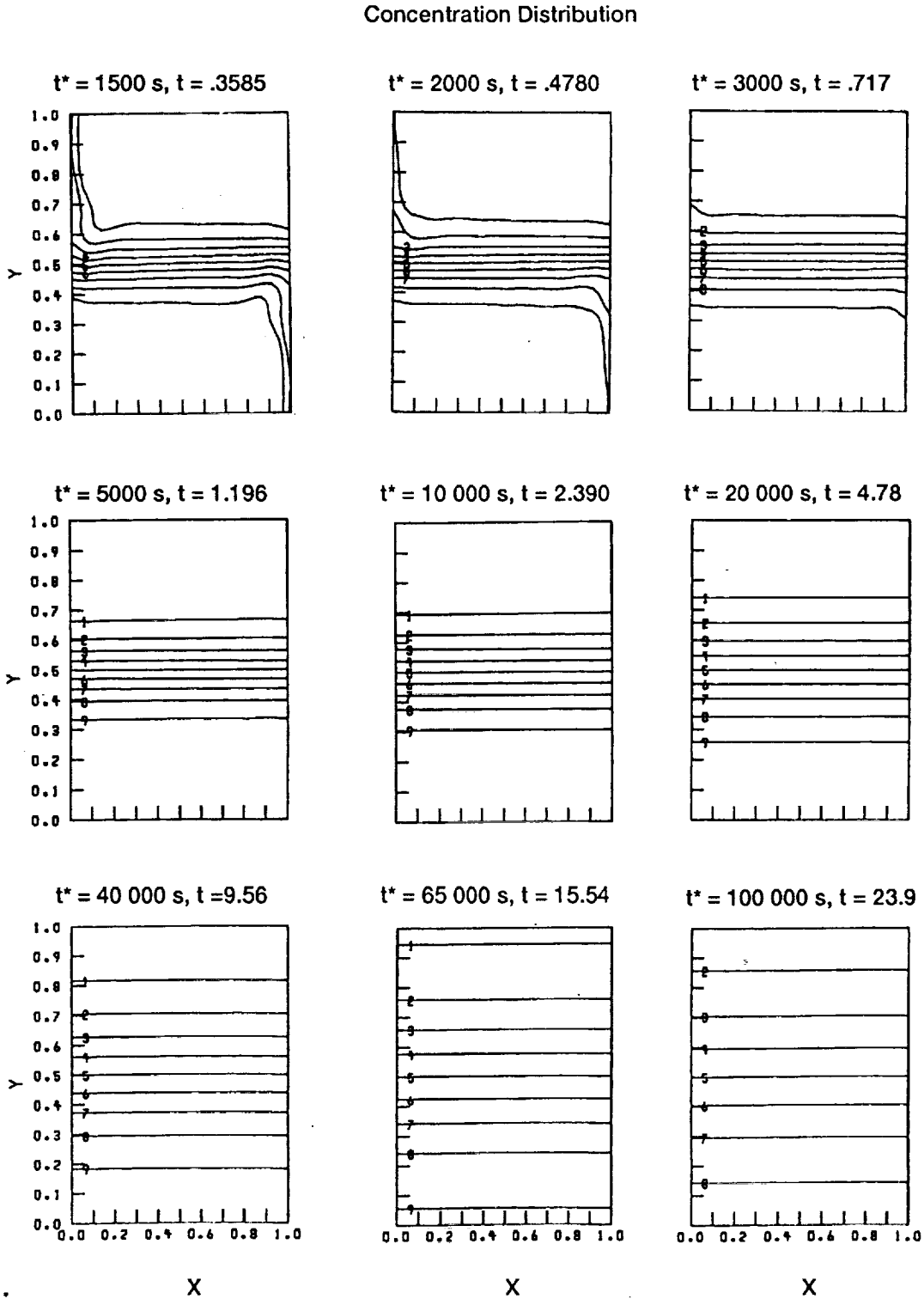

Figure 2(d).—Mixing of stably stratified fluids.

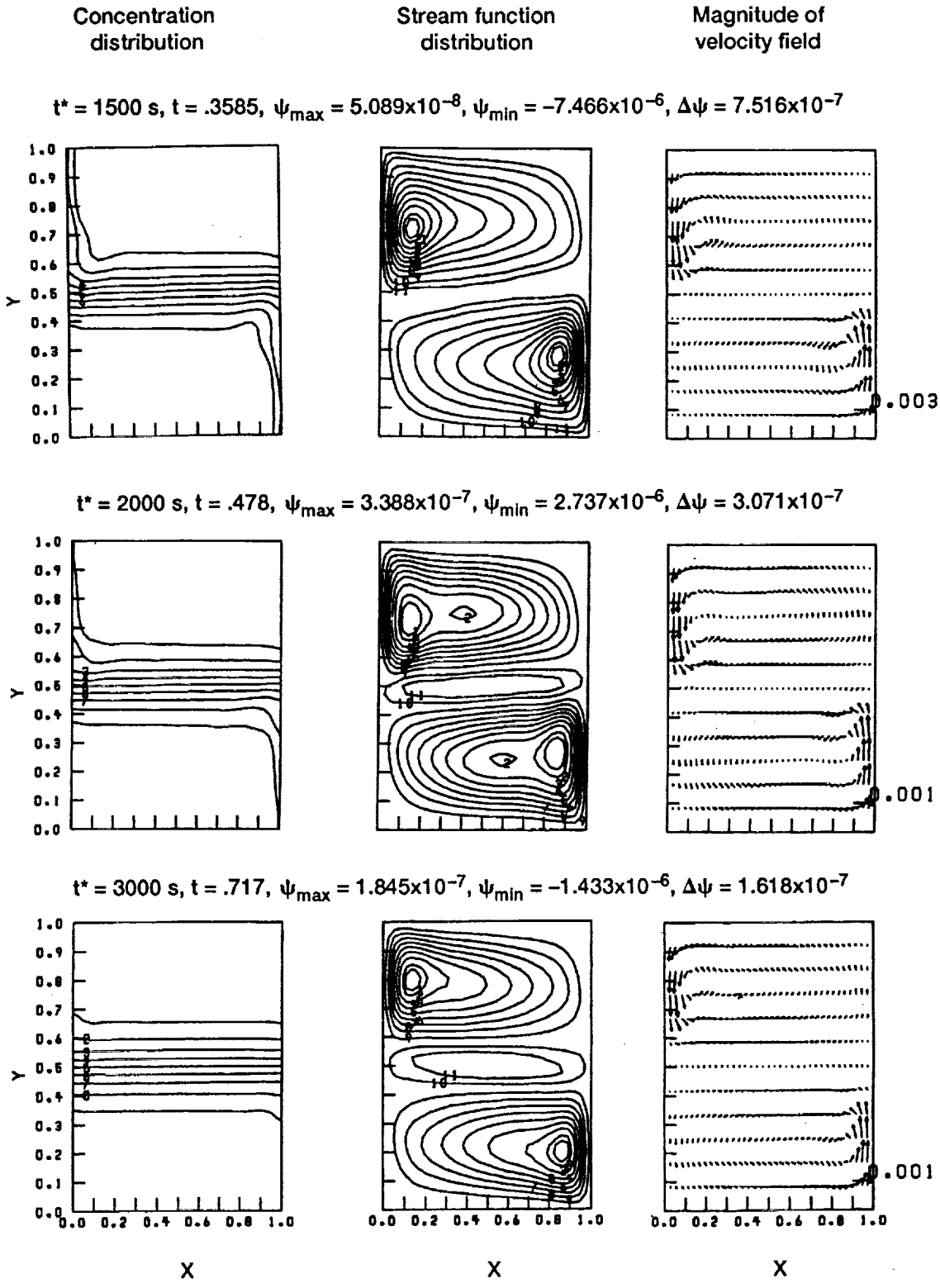

Figure 2(e).—Characteristics of the flow field during mixing, viscous diffusion time scale.

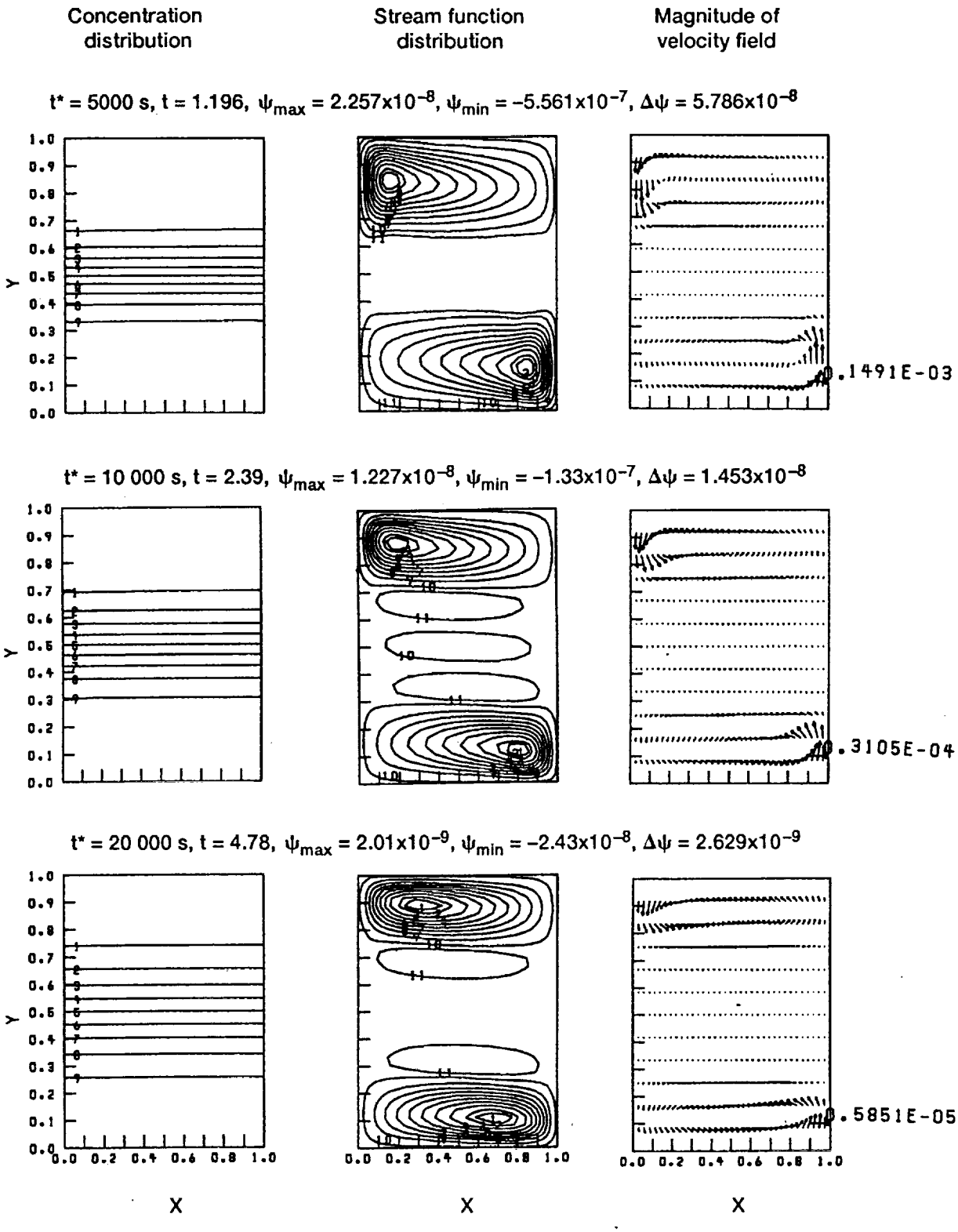

Figure 2(f).—Characteristics of the flow field during mixing, transition to mass diffusion time scale.

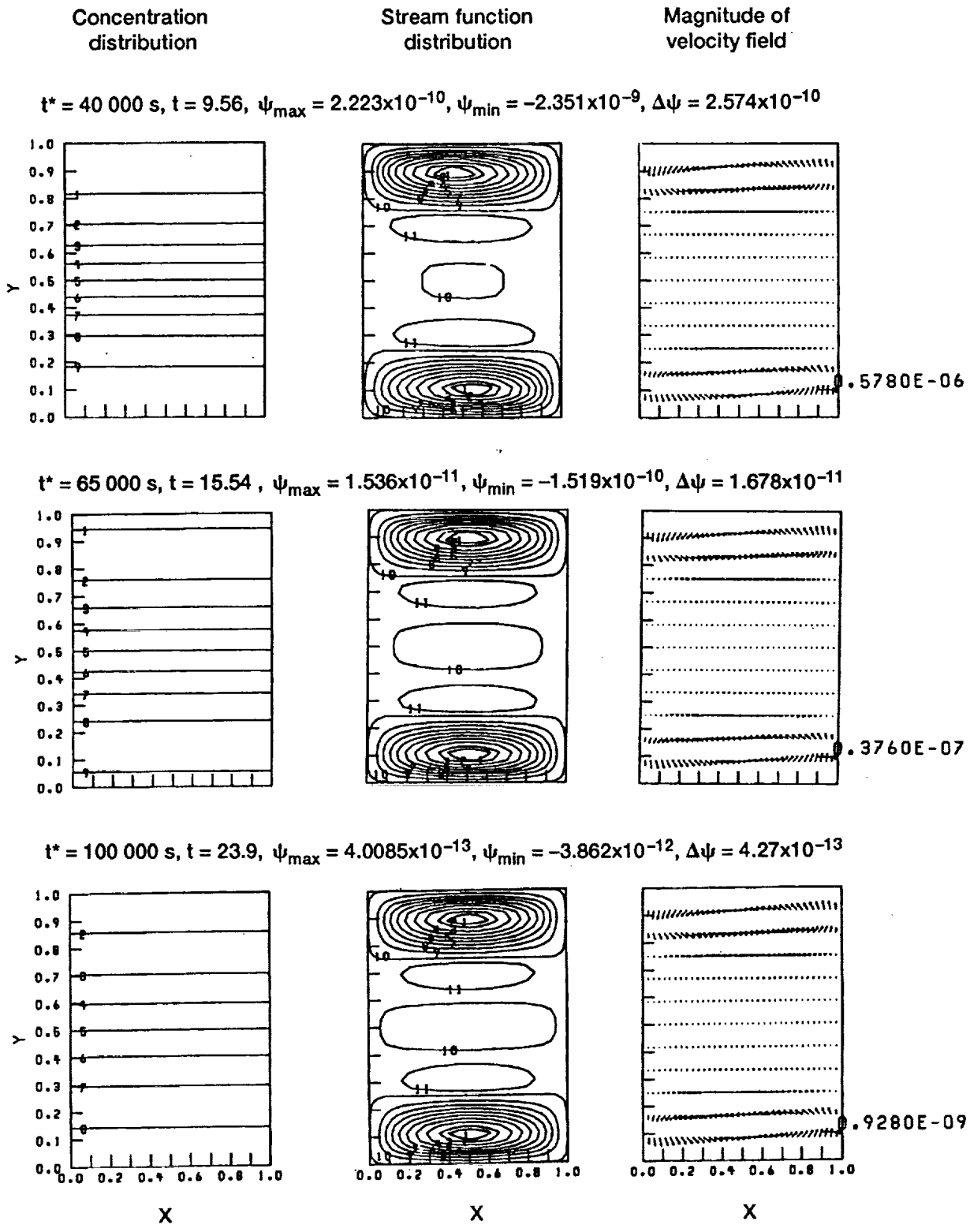

Figure 2(g).—Characteristics of the flow field during mixing, decay to equilibrium. For the magnitude of vector field plot, the bottom numerical value represents the magnitude of the flow field $V_{mag/.8}$ = x cm/sec.

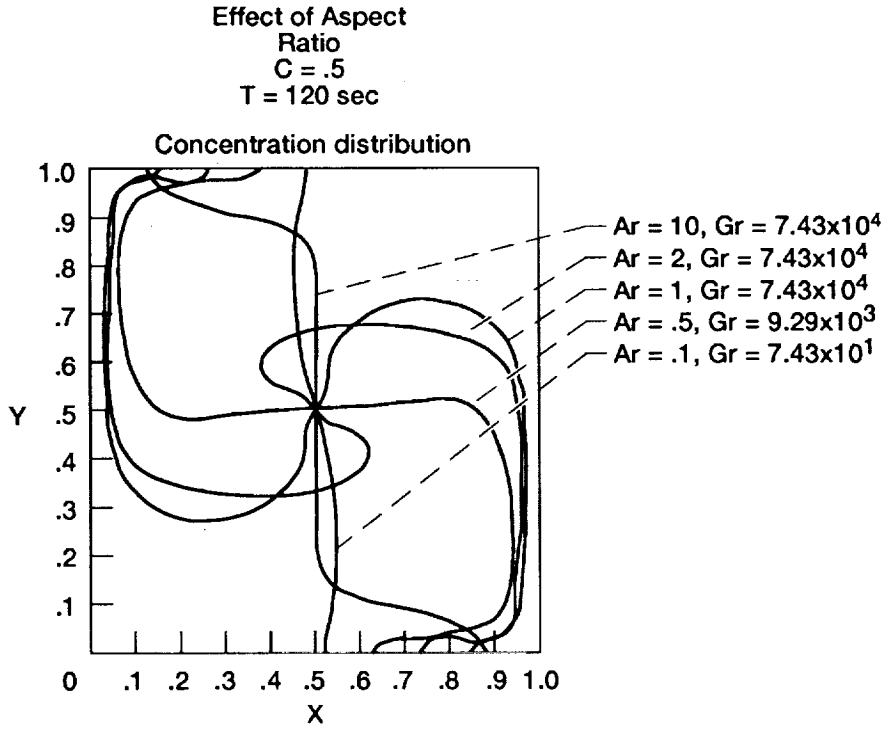

Figure 3.—Effect of aspect ratio, corresponding material interface.

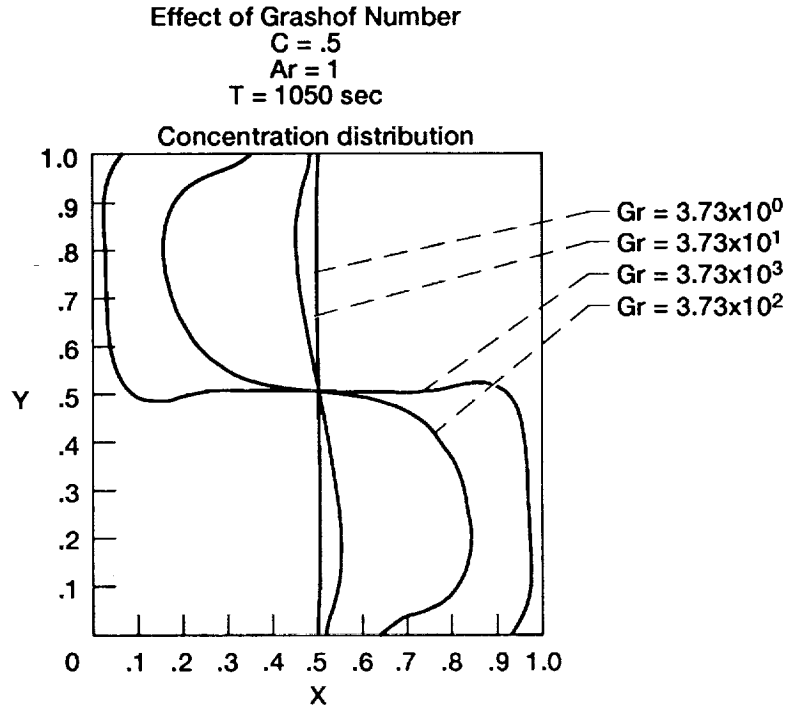

Figure 4.—Effect of Grashof number and corresponding material interface.

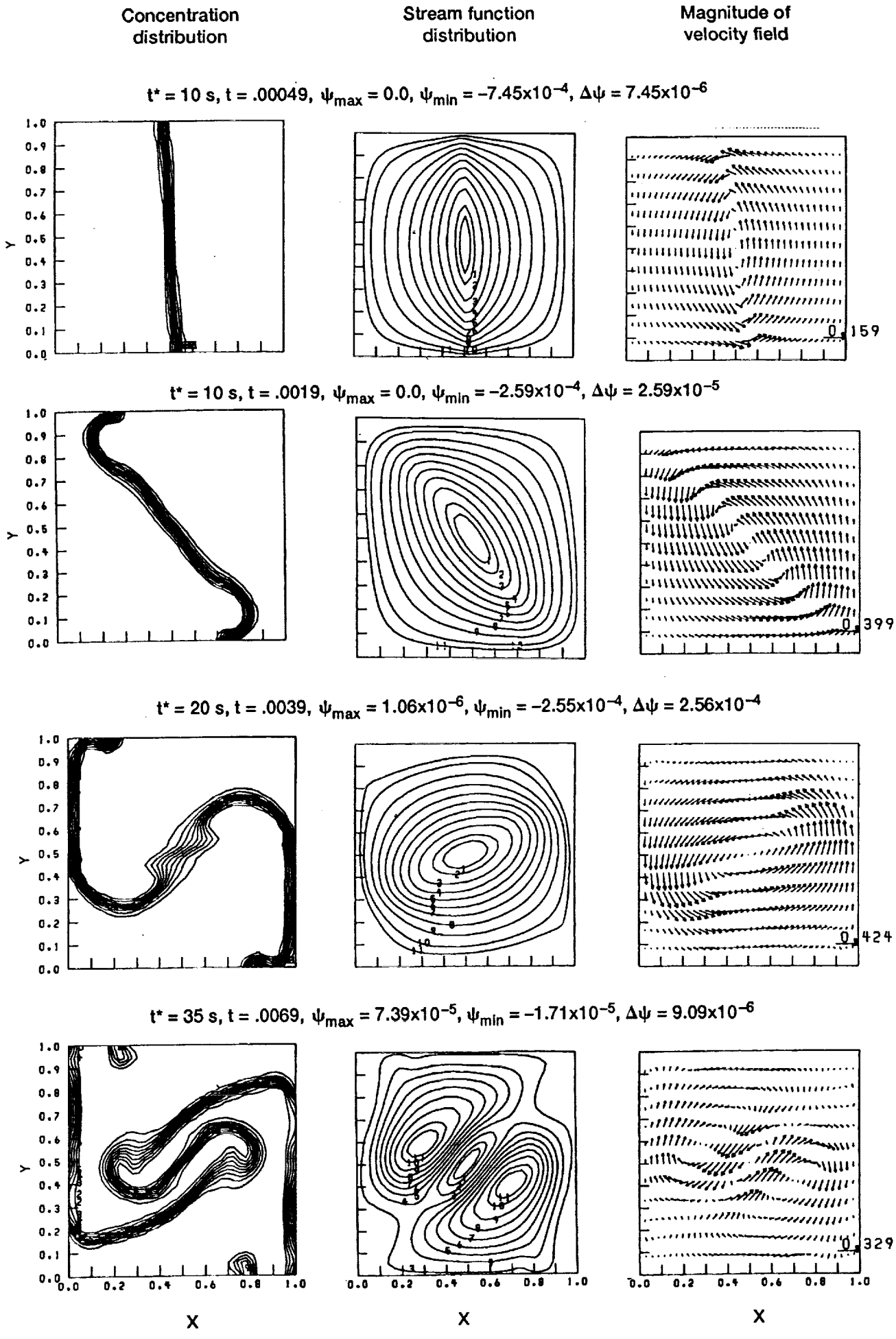

Figure 5(a).—Early time evolution of internal breakwave.

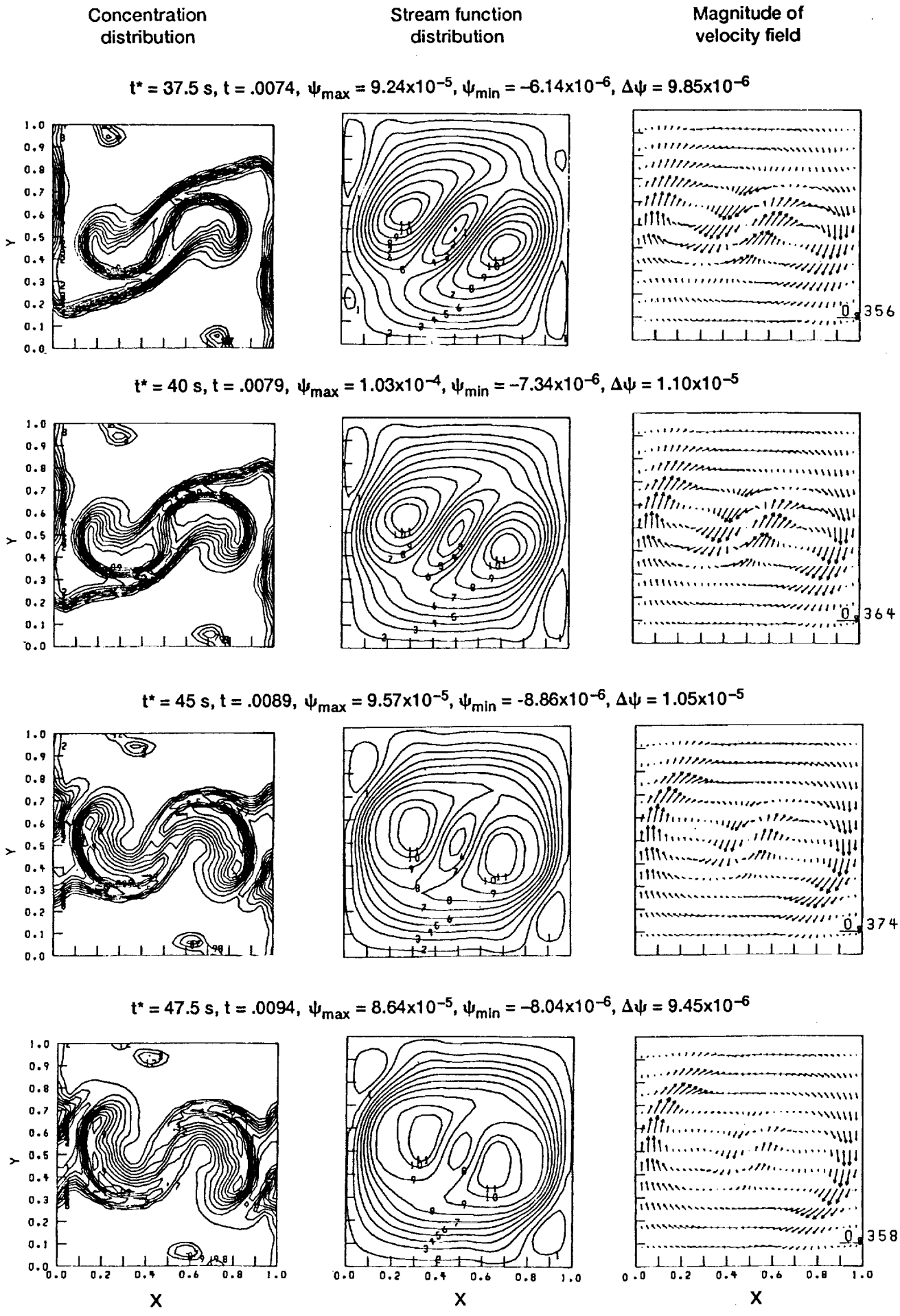

Figure 5(b).—Wavebreaking, droplet formation and detachment.

Concentration distribution | Stream function distribution | Magnitude of velocity field

$t^* = 67.5$ s, $t = .013$, $\psi_{max} = 0.0$, $\psi_{min} = -4.26 \times 10^{-5}$, $\Delta\psi = 4.26 \times 10^{-6}$

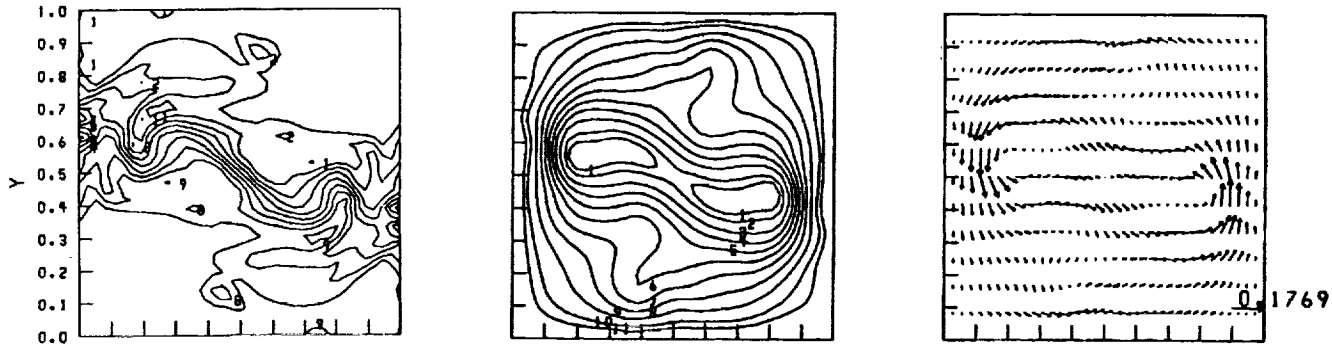

$t^* = 300$ s, $t = .059$, $\psi_{max} = 0.0$, $\psi_{min} = -6.09 \times 10^{-6}$, $\Delta\psi = 6.09 \times 10^{-7}$

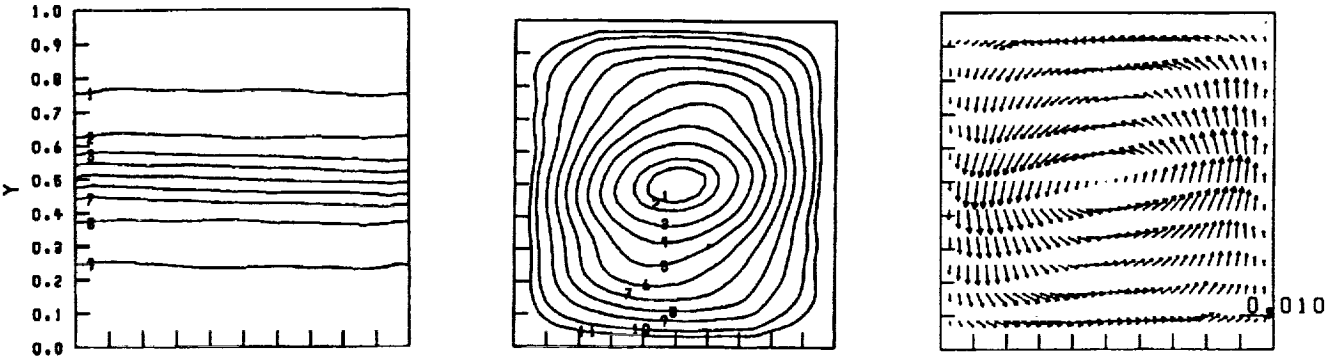

$t^* = 630$ s, $t = .124$, $\psi_{max} = 2.15 \times 10^{-7}$, $\psi_{min} = -1.27 \times 10^{-7}$, $\Delta\psi = 3.42 \times 10^{-8}$

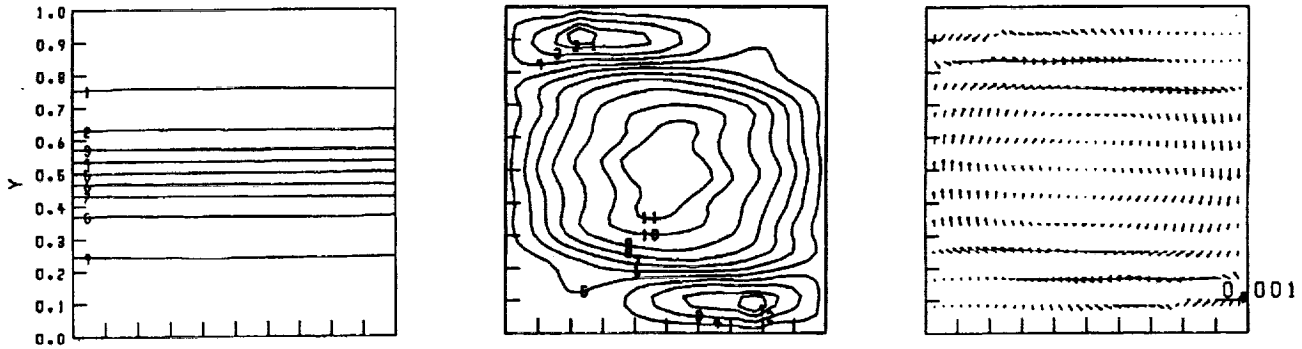

$t^* = 1050$ s, $t = .207$, $\psi_{max} = 9.51 \times 10^{-9}$, $\psi_{min} = -6.58 \times 10^{-8}$, $\Delta\psi = 7.53 \times 10^{-9}$

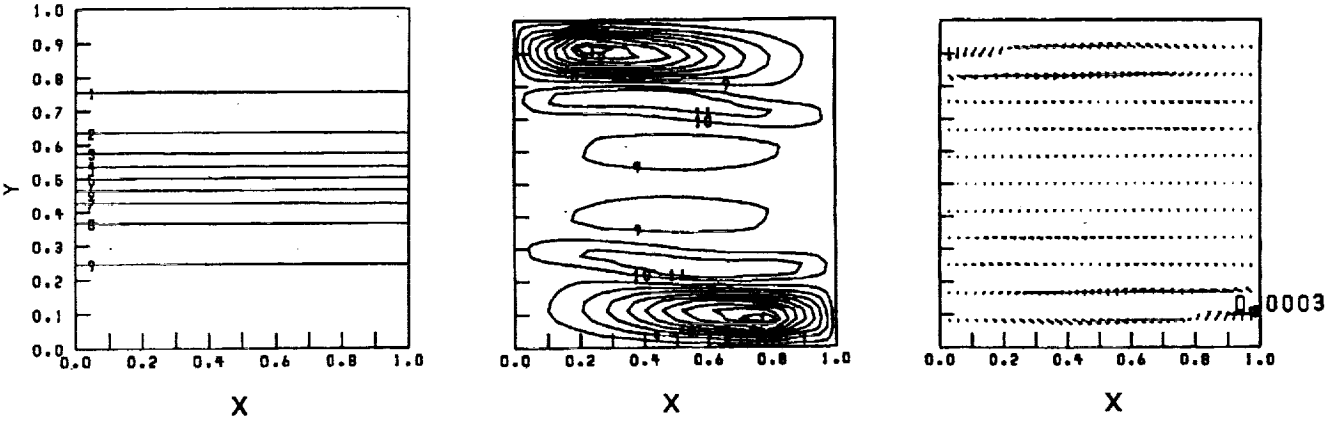

Figure 5(c).—Droplet reattachment and stratification.

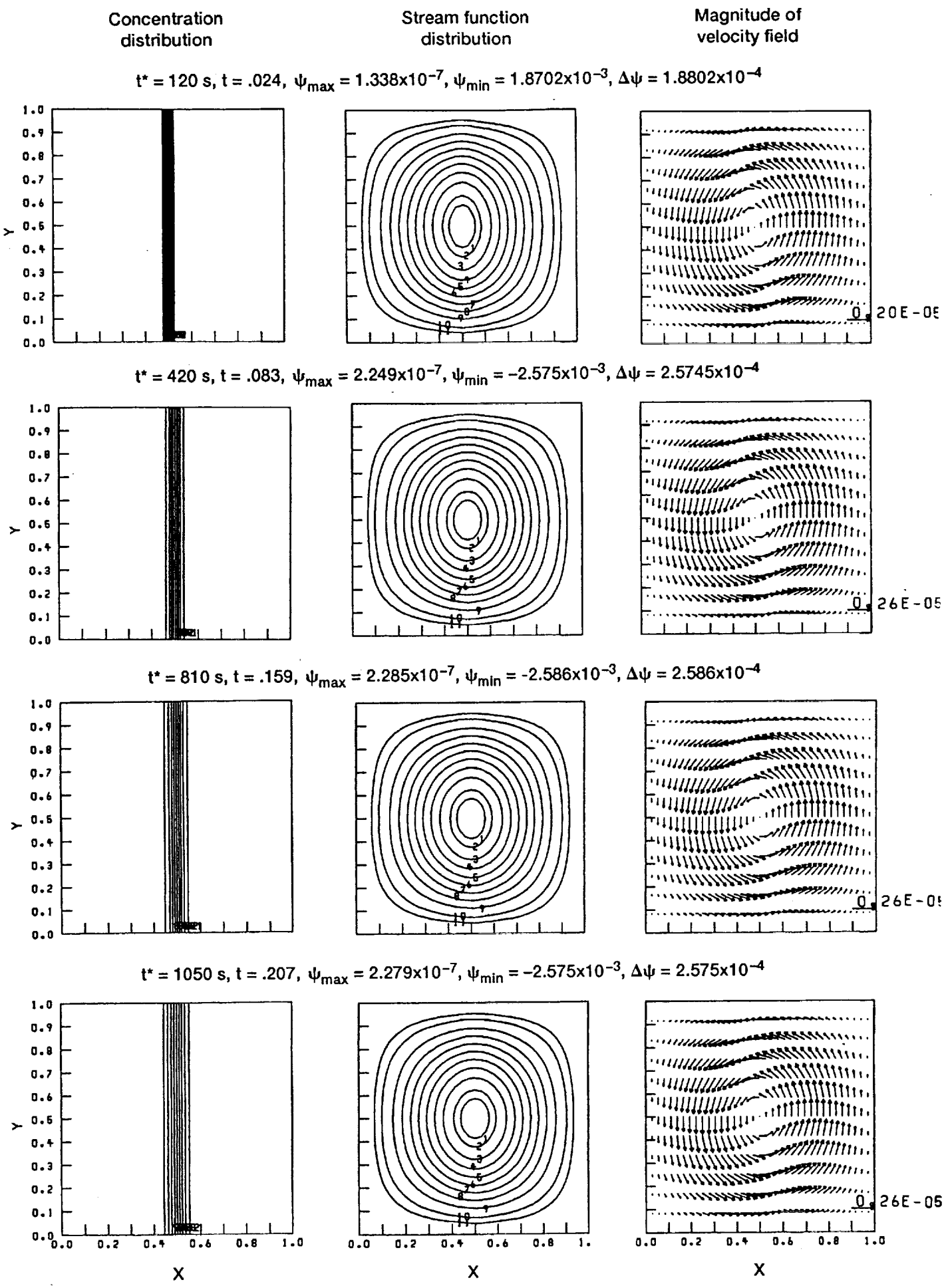

Figure 6.– Diffusive mixing, Gr = .37, Ar = 1, and Sc = 247.

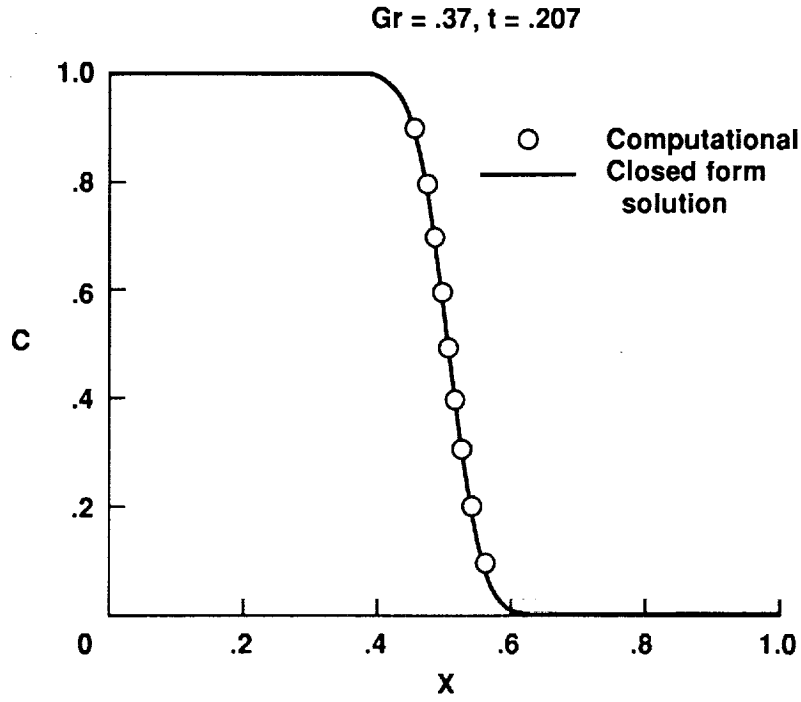

Figure 7.—Comparison of closed form solution to computational results.

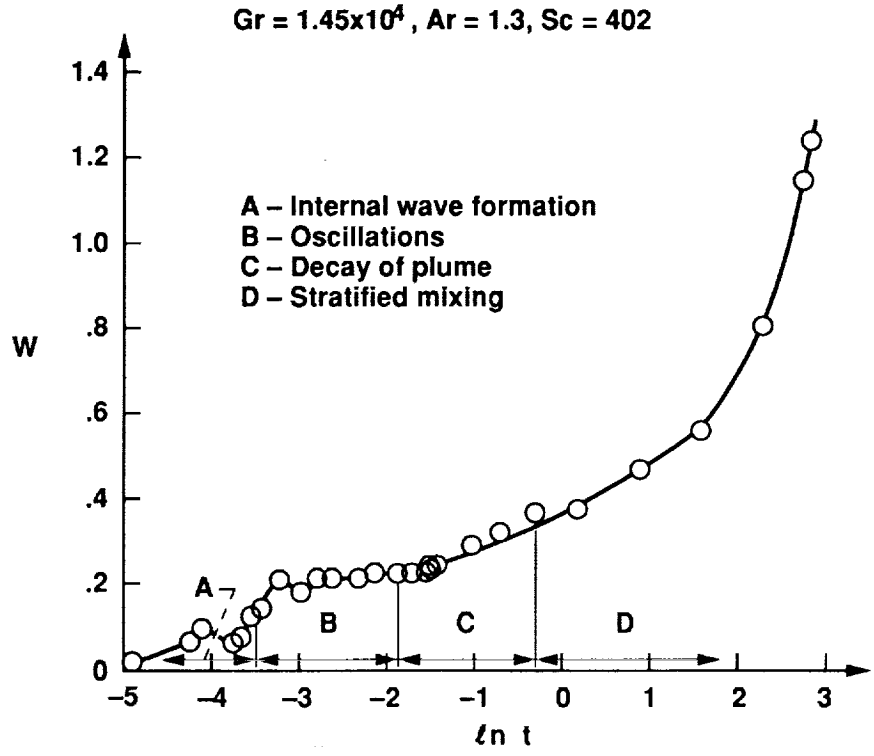

Figure 8.—Interface width as a function of time for the convective regime.

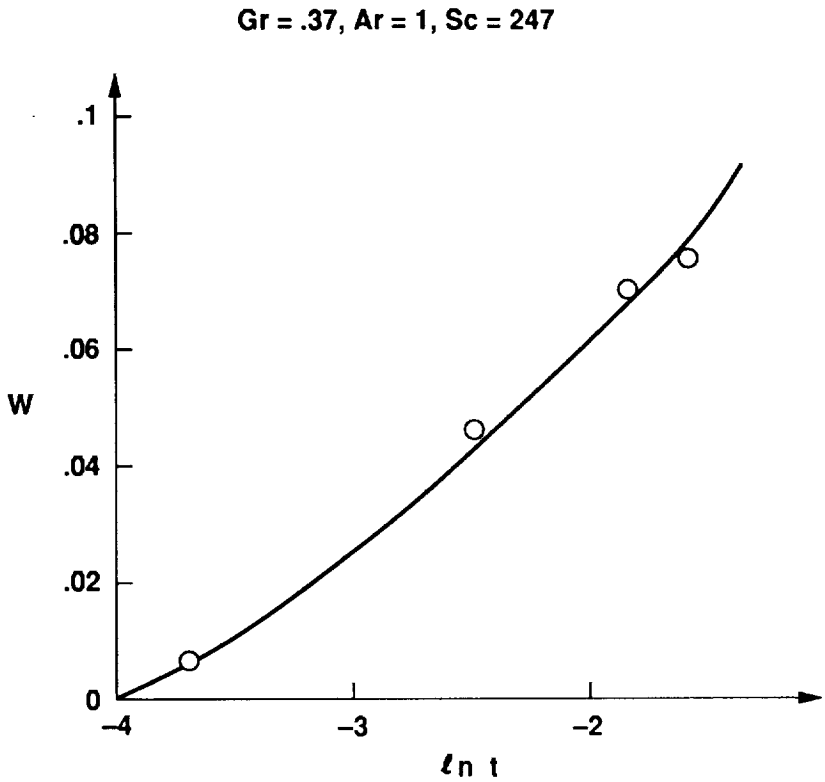

Figure 9.—Interface width as a function of time for the diffusive regime.

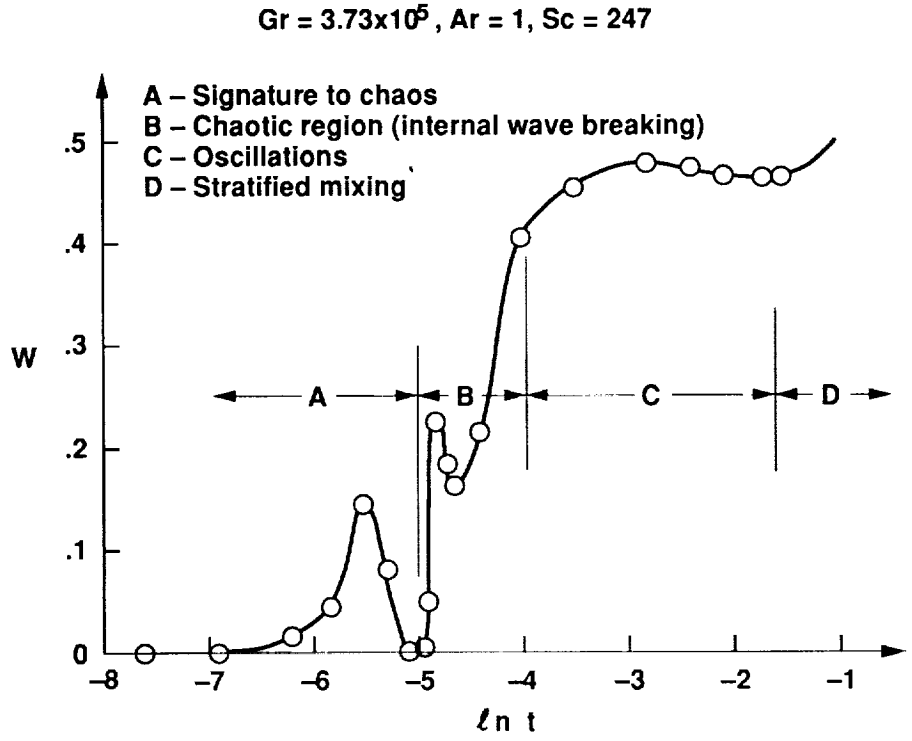

Figure 10.—Interface width as a function of time for the chaotic regime.

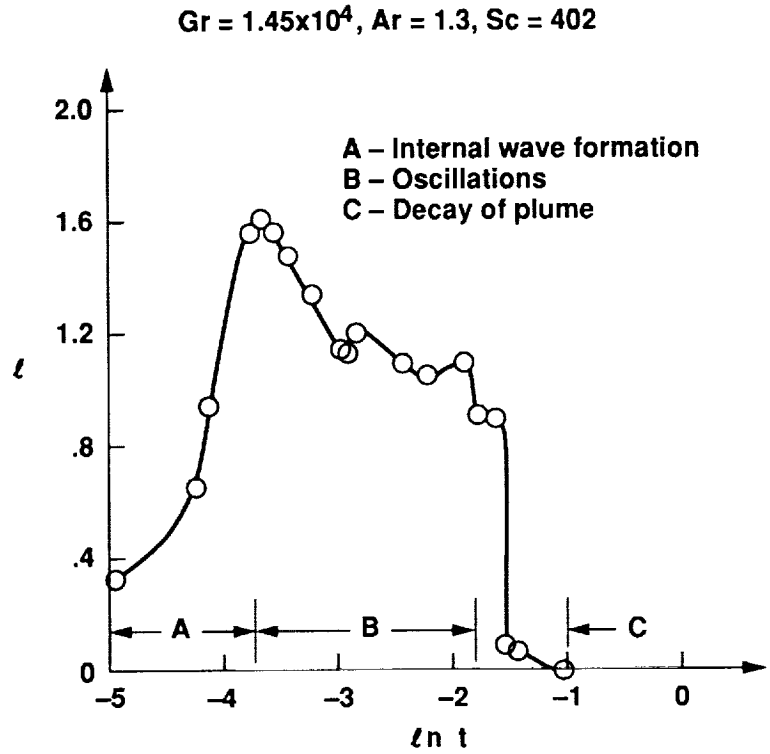

Figure 11.—Interface elongation as a function of time for the convective regime.

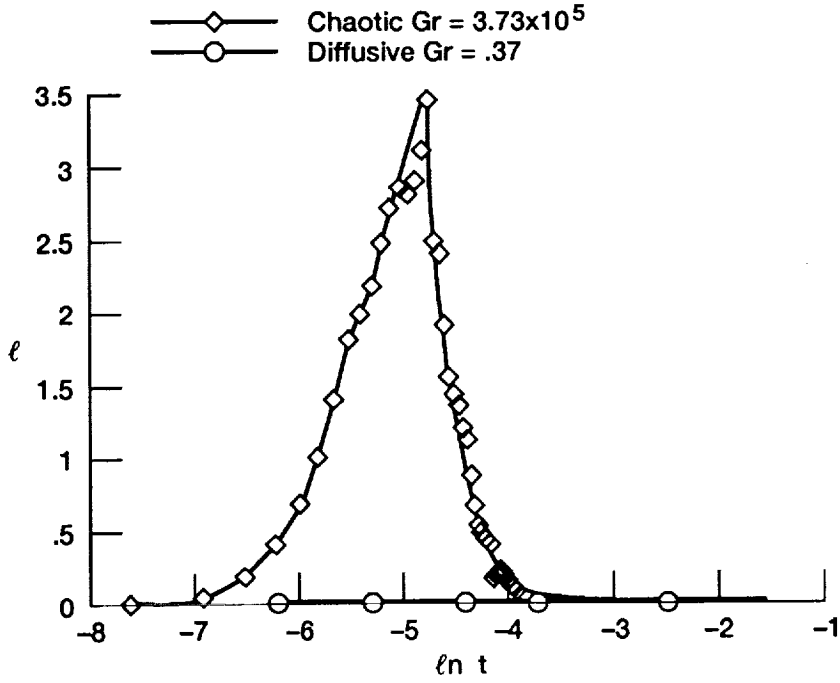

Figure 12.—Interface elongation as a function of time for the diffusive and chaotic regime.

REPORT DOCUMENTATION PAGE

Form Approved
OMB No. 0704-0188

Public reporting burden for this collection of information is estimated to average 1 hour per response, including the time for reviewing instructions, searching existing data sources, gathering and maintaining the data needed, and completing and reviewing the collection of information. Send comments regarding this burden estimate or any other aspect of this collection of information, including suggestions for reducing this burden, to Washington Headquarters Services, Directorate for information Operations and Reports, 1215 Jefferson Davis Highway, Suite 1204, Arlington, VA 22202-4302, and to the Office of Management and Budget, Paperwork Reduction Project (0704-0188), Washington, DC 20503.

1. AGENCY USE ONLY (*Leave blank*)	2. REPORT DATE	3. REPORT TYPE AND DATES COVERED
	October 1992	Technical Memorandum

4. TITLE AND SUBTITLE

Numerical Study of Mixing of Two Fluids Under Low Gravity

5. FUNDING NUMBERS

WU-674-21-05

6. AUTHOR(S)

Walter M.B. Duval

7. PERFORMING ORGANIZATION NAME(S) AND ADDRESS(ES)

National Aeronautics and Space Administration
Lewis Research Center
Cleveland, Ohio 44135-3191

8. PERFORMING ORGANIZATION REPORT NUMBER

E-7326

9. SPONSORING/MONITORING AGENCY NAMES(S) AND ADDRESS(ES)

National Aeronautics and Space Administration
Washington, D.C. 20546-0001

10. SPONSORING/MONITORING AGENCY REPORT NUMBER

NASA TM-105865

11. SUPPLEMENTARY NOTES

Responsible person, Walter M.B. Duval, (216) 433-5023.

12a. DISTRIBUTION/AVAILABILITY STATEMENT

Unclassified - Unlimited
Subject Category 34 and 64

12b. DISTRIBUTION CODE

13. ABSTRACT (*Maximum 200 words*)

The mixing characteristic of two fluids inside a cavity due to buoyancy driven flow fields for low gravity conditions is investigated via numerical experiments. The buoyancy driven flow, depending on the parametric region, stretches and deforms the material interface into a wave morphological pattern. The morphological pattern affects the resulting stratification thickness of the mixed region. Three basic mixing regimes occur: convective, diffusive, and chaotic. In the convective regime, an overturning motion occurs which gives rise to a stable wave formation. This wave oscillates and its decay leads to a stable stratification. Whereas, in the diffusive regime, the length of the interface remains constant while mixing occurs. This limiting behavior is very important to materials processing in space, and it admits a closed form solution corresponding to vanishing convective terms which agrees with computational results. Finally in the chaotic regime, the material interface continuously stretches and folds on itself similar to a horseshoe map. The length of stretch of the interface increases exponentially. Internal wavebreaking occurs for this case. This wavebreaking generates local turbulence, and provides an effective mechanism for mixing.

14. SUBJECT TERMS

Mixing; Buoyancy flow fields; Low gravity; Mass transport; Internal wavebreazing; Chaos; Convection

15. NUMBER OF PAGES

44

16. PRICE CODE

A03

17. SECURITY CLASSIFICATION OF REPORT	18. SECURITY CLASSIFICATION OF THIS PAGE	19. SECURITY CLASSIFICATION OF ABSTRACT	20. LIMITATION OF ABSTRACT
Unclassified	Unclassified	Unclassified	